

## Research article

# Synthesis of a new quaternary ammonium salt for efficient inhibition of mild steel corrosion in 15 % HCl: Experimental and theoretical studies

Lipiar K.M.O. Goni<sup>a</sup>, Shaikh A. Ali<sup>a,b</sup>, Hasan A. Al-Muallem<sup>a,c</sup>, Mohammad A. Jafar Mazumder<sup>a,b,\*</sup>

<sup>a</sup> Chemistry Department, King Fahd University of Petroleum & Minerals, Dhahran 31261, Saudi Arabia

<sup>b</sup> Interdisciplinary Research Center for Refining and Advanced Chemicals, King Fahd University of Petroleum & Minerals, Dhahran 31261, Saudi Arabia

<sup>c</sup> Interdisciplinary Research Center for Advanced Materials, King Fahd University of Petroleum & Minerals, Dhahran 31261, Saudi Arabia

## ARTICLE INFO

## Keywords:

Quaternary ammonium salt  
15 % HCl  
Mild steel  
Corrosion inhibition  
Inhibitor adsorption  
Acidizing corrosion

## ABSTRACT

The corrosion phenomenon and its economic impacts can hardly be ignored in any application. This study synthesized a quaternary ammonium salt (**3**) containing hydrophobic dodecyl and electron-rich diallylbenzyl amine moieties to be used in 15 % HCl as a corrosion inhibitor of mild steel. Several techniques, such as <sup>1</sup>H and <sup>13</sup>C NMR, IR, TGA, and elemental analysis, have been used to characterize inhibitor **3**. Popular corrosion measurement techniques, namely weight loss, potentiodynamic polarization techniques, and electrochemical impedance spectroscopy, have been used to determine the efficiency of inhibitor **3**. At 303 K and a moderately low concentration of 50 ppm, the quaternary ammonium salt-based inhibitor demonstrated a maximum efficiency of  $\approx 95.0$  %. At elevated temperatures of 313, 323, and 333 K, the inhibition efficacy values were recorded as 91.3, 82.8, and 75.0 %, respectively. Adsorption isotherm study revealed that the adsorption of inhibitor **3** followed Langmuir adsorption isotherm. The value of  $\Delta G_{ads}^{\circ}$  was found to be  $-40.19$  kJ mol<sup>-1</sup>, indicating that inhibitor **3** became adsorbed via a mixed physichemisorption mechanism. A very high adsorption constant ( $K_{ads}$ ) of  $1.53 \times 10^5$  L mol<sup>-1</sup> suggested strong adsorption of inhibitor **3**. The difference in activation energy ( $E_a$ ) value of 42.4 kJ mol<sup>-1</sup> between the control and the inhibited solution indicated an efficient adsorption of inhibitor **3**. The ability of inhibitor **3** to retard both anodic and cathodic half-cell reactions was proved via open circuit potential and Tafel curves studies. Detailed discussions on the change in corrosion current densities ( $i_{corr}$ ), polarization ( $R_p$ ) and charge transfer ( $R_{ct}$ ) resistances have been offered to discuss the inhibition efficiency. Water contact angle measurement showed a drastic increase in mild steel surface hydrophobicity following inhibitor **3** adsorption. SEM-EDX and XPS studies confirmed the definitive presence of inhibitor **3** on the mild steel surface. Density functional theory (DFT) studies revealed the frontier molecular orbitals with which the metal surface interacts. A detailed corrosion inhibition mechanism has been offered in the context of adsorption isotherm and DFT studies.

\* Corresponding author.

E-mail address: [jafar@kfupm.edu.sa](mailto:jafar@kfupm.edu.sa) (M.A. Jafar Mazumder).

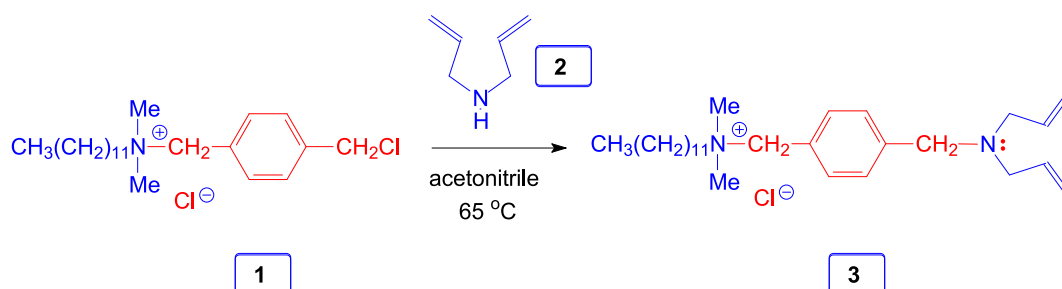
## 1. Introduction

Corrosion is an electrochemical process that causes the metal to degrade when it's in contact with a corrosive medium, forcing it to undergo mass and charge transfer simultaneously [1]. The menaces of corrosion are so pervasive that corrosion-related costs account for  $\approx 5\text{--}7\%$  of any nation's GNP [2]. Owing to strength and affordability, low-carbon steel, containing carbon in the range of 0.05–0.3 %, has seen myriad applications for industrial and engineering purposes [3]. In oil and gas industries, acidizing technology is very crucial to increasing oil and gas production. Generally, concentrated acids, 15–28 % HCl in general, are flushed into the reservoir through the wellbore, and these acids crush the clay minerals and carbonate rocks. This causes the reservoir permeability to increase and the flow paths to improve, thereby enhancing oil recovery [4]. Unfortunately, because they are highly corrosive, acids cause severe damage to downhole metallic equipment, resulting in economic losses of various magnitudes.

A recent study by the NACE demonstrated that the global cost of corrosion equated to 3.4 % of the worldwide GDP in 2013 [5]. The current corrosion cost can be reduced by 15–35 %, equating to 375–875 US billion dollars, using the available anticorrosion methods [6]. One prevalent, economical, and easy-to-use approach is corrosion inhibitors [7]. Corrosion inhibitors, as the name implies, are chemical compounds that, when added/used in meager concentrations, can significantly reduce the metal dissolution rate. Small molecules or organic compounds are widely used to mitigate the corrosion of steels in acidic media [8]. Organic compounds contain different functionalities and experience chemical/electrostatic interactions or a combination of both with the metal surface in solution. Therefore, these molecules having N, O, S, and P heteroatoms, aromatic rings,  $\pi$ -systems, conjugated bonds, polar functional groups ( $-\text{NO}_2$ ,  $-\text{NH}_2$ ,  $-\text{COOH}$ ,  $-\text{OH}$ ,  $-\text{CN}$ ,  $-\text{C}=\text{O}$ ), etc., are considered effective corrosion inhibitors.

Quaternary ammonium compounds effectively counter the corrosion of metals and other underground pipelines in acidic media [9, 10]. The quaternary ammonium moiety is advantageous and can be decorated with different functionalities to tailor and improve the inhibition efficiency. Moreover, different alkyl chain lengths and hydrophobic motifs can be incorporated into quaternary ammonium compounds, which have proven useful [11,12]. To counter the corrosion of carbon steel in 1 M HCl, Chauhan et al. [13] studied the anticorrosion properties of a tripropylamine-based quaternary salt. At a high concentration of 200 ppm, the inhibitor showed a maximum inhibition efficiency (IE) of 93 %. A quaternary ammonium salt surfactant corrosion inhibitor was used by Jalab et al. [14] to study the corrosion of carbon steel in 5 M HCl. At a concentration of 2.22 mM, the inhibitor achieved a low IE of 56.0 %. To inhibit mild steel corrosion in 1 M HCl, Haque et al. [11] studied the IE of three propargyl pyrrolidinium bromide quaternary ammonium salts (DPPB, DDPPB, and HDPPB). For a small concentration of 60.3  $\mu\text{M}$ , DPPB, DDPPB, and HDPPB showed excellent IEs of 92.6, 93.7, and 96.2 %, respectively. Tabei et al. [15] used a bis-cationic surfactant to retard carbon steel corrosion in 1 M HCl. It was found to inhibit the corrosion of carbon steel by 94.7 % at a concentration of  $1 \times 10^{-3}$  M. The anti-corrosive effects of dodecyl trimethyl ammonium bromide and thiourea mixture (DTAB-Thiourea) and dodecyl dimethyl benzyl ammonium bromide (DDBAB-Thiourea) were studied for Q235 steel corrosion in 0.05 mol L<sup>-1</sup> [16]. DTAB-Thiourea and DDBAB-Thiourea inhibited the corrosion of Q235 steel by 93.37 and 94.98 %, respectively.

Mild steel has seen tremendous applications because of its extraordinary mechanical strength, easy availability, and low cost. It is extensively used across many industries for fabrication and construction. However, when subjected to different organic and inorganic acids during chemical or electrochemical processes in oil refineries and shipbuilding, as well as during acid cleaning, pickling, and metals descaling, mild steel suffers from severe corrosion [17,18]. Therefore, it's imperative that new corrosion inhibitors must be synthesized to be used in extremely harsh acid conditions. In this study, we synthesized a new quaternary ammonium chloride salt (**3**) (Scheme 1) containing a diallyl amine moiety with unquenched nitrogen, a benzene ring with  $\pi$ -electrons, and a favorable alkyl chain length to promote hydrophobicity on the mild steel surface. To the best of our knowledge, this is the first instance of this compound being reported. The proposed inhibitor has a good balance of hydrophobicity in the form of an alkyl chain moiety and hydrophilicity in the form of a quaternary ammonium salt moiety. As such, the inhibitor demonstrated an excellent IE tested via several corrosion measuring techniques. A very high inhibition efficiency of 95.2 % was registered for just 0.1 mM inhibitor concentration, which is rare in literature (vide infra, see Table 7). Following very efficient adsorption of inhibitor **3**, several surface characterization techniques were employed to prove the adsorption of inhibitor **3**. DFT-based computational studies have also been performed to develop knowledge of the inhibitor sites that establish chemical communication with the metal surface.



Scheme 1. Synthesis of inhibitor molecule 3.

## 2. Experimental

### 2.1. Materials

The quaternary ammonium compound (**1**) was synthesized following a work reported earlier [19]. Diallylamine (**2**) was acquired from Sigma-Aldrich and used as obtained. The metal samples (mild steel specimens) were obtained from Chrome Royal Al Arabian Contracting Ltd, Riyadh, Saudi Arabia, as a gift. All the solvents (analytical grade) required for this study were bought from Sigma-Aldrich and used as they arrived. The used mild steel samples were of the composition (wt.%): C (0.21 %), P (0.06 %), Si (0.29 %), Cu (0.06 %), S (0.05 %), Mn (0.49 %), and Fe (balance). The corrosive medium (the electrolyte test solution) was 15 % HCl, prepared by diluting 37 % HCl with deionized water.

### 2.2. Physical methods

A PerkinElmer (2400 Series II) CHNS/O elemental analyzer was used to find out the atomic compositions of inhibitor **3**. A PerkinElmer 16 PC FTIR spectrometer was used to record the IR spectra.  $\text{CDCl}_3$  was used as the solvent to record  $^1\text{H}$  and  $^{13}\text{C}$  NMR spectra using a 400-MHz Bruker Avance III spectrometer. TMS and  $^{13}\text{C}$   $\text{CDCl}_3$  signals at  $\delta$  0 and 77.0 ppm were used as references, respectively. Thermogravimetric analysis (TGA) of **3** was carried out using SDT Q600 developed by the TA Instruments. Thermal stability of **3** was conducted under  $\text{N}_2$  flow ( $50 \text{ mL min}^{-1}$ ) condition. The TGA curves were recorded from  $20^\circ\text{C}$  until  $800^\circ\text{C}$ , increasing the temperature by  $10^\circ\text{C}$  per minute.

### 2.3. Synthesis of inhibitor molecule 3

The synthesis route for preparing inhibitor molecule **3** is presented as Scheme 1. Briefly, in 25 mL acetonitrile, a solution of **1** (3.88 g, 10.0 mmol) and **2** (4.86 g, 50 mmol) was stirred under  $\text{N}_2$  at  $65^\circ\text{C}$  for 24 h. Following the removal of the solvent and remaining diallyl amine **2**, 20 mL of deionized water was used to dissolve the remainder of the mixture, followed by treating with NaOH (500 mg, 12.5 mmol). Afterward, the aqueous layer was extracted with three portions (50 mL each) of diethyl ether. A saturated NaCl solution (20 mL) was used to wash the organic layer before drying it over  $\text{Na}_2\text{SO}_4$ . Diethyl ether was removed, and the residue was dried under vacuum at  $60^\circ\text{C}$ , which afforded inhibitor compound **3** as a light-yellow semisolid (4.27 g, 95 %).

### 2.4. Corrosion studies

#### 2.4.1. Gravimetric weight loss

To conduct the gravimetric WL tests, mild steel coupons ( $2.8 \text{ cm} \times 2.8 \text{ cm} \times 0.6 \text{ cm}$ ) were prepared and cleaned following ASTM standards (ASTM G31-21). After taking their weight, mild steel coupons were immersed in 15 % HCl solution with and without inhibitors in 250 mL Wheaton bottles filled up to 200 mL. The coupons were allowed to corrode in the absence and presence of **3** (1, 5, 10, 20, 50, and 100 ppm) for 3 h at  $30^\circ\text{C}$  (303 K). The weight loss tests at each temperature were triplicated, and the mean value was used to calculate the IEs. After 3 h, the coupons were taken out of the bottles. The corrosion products on the coupons were cleaned following the ASTM mentioned above standards. After that, the final weight of the coupons was measured after they were dried. To facilitate thermodynamics studies, additional WL tests were conducted at 313, 323, and 333 K. Eq. (1) was used to calculate the IEs imparted by different concentrations of **3** and Eq. (2) to calculate the corrosion rates (CR).

$$\eta_{\text{WL}} (\%) = \frac{W_o - W_i}{W_o} \times 100 \quad (1)$$

$$\text{CR} (\text{mmy}^{-1}) = \frac{87.6 \times \Delta W}{\text{DAT}} \quad (2)$$

Where,  $W_o$  and  $W_i$  represent weight losses in the absence and presence, respectively, of inhibitor **3**,  $\Delta W = W_b - W_a$ , where  $W_b$  and  $W_a$  depict the weight of mild steel coupons before and after immersion, respectively,  $D$  is the density of Fe in mild steel ( $7.87 \text{ g cm}^{-3}$ ),  $A$  is the exposed coupon area, and  $T$  is the immersion time (3 h). The area of the metal coupons was calculated using the formula:  $2[(\text{length} \times \text{width}) + (\text{width} \times \text{height}) + (\text{height} \times \text{length})]$ , with the dimensions being measured in cm.

#### 2.4.2. Electrochemical corrosion study

The electrochemical studies were conducted using a Gamry three-electrode electrochemical cell in a static condition at  $30^\circ\text{C}$ . A graphite rod, a piece of mild steel, and a standard calomel electrode (SCE) were used as the counter, working, and reference electrodes. The electrochemical cell can accommodate 300 mL testing solutions and is designed to expose only a  $1 \text{ cm}^2$  working electrode (mild steel) area to the testing solutions. A Gamry Reference 3000 Potentiostat/Galvanostat/ZRA was used to conduct electrochemical corrosion studies, and the electrochemical cell was connected to it. The Gamry framework system (ESA410) associated with the Gamry Reference 3000 was utilized to record the impedance and polarization curves. The recorded curves were fitted using Echem Analyst software (version: 7.8.2) developed by Gamry to derive relevant electrochemical parameters. Before each measurement, the open circuit potential ( $E_{\text{OCP}}$ ) was recorded for 1 h to allow the system to gain a stable potential. EIS measurements were carried out in the 10 kHz to 10 mHz frequency range using a small, 10 mV AC perturbation. The IEs from EIS measurements ( $\eta_{\text{EIS}}\%$ ) were calculated using

Eqs. (3) and (4).

$$\eta_{EIS}(\%) = \left(1 - \frac{R_{ct}^{\circ}}{R_T}\right) \times 100 \quad (3)$$

$$R_T = R_{ct} + R_{fm} \quad (4)$$

Where,  $R_{ct}^{\circ}$  and  $R_{ct}$  represent charge transfer resistance in the absence and presence of the inhibitor, respectively,  $R_{fm}$  means the film resistance arising from the adsorption of the inhibitor and  $R_T$  stands for total resistance.

At a scan rate of 0.5 mV/s, the mild steel surface was polarized by  $\pm 250$  mV against the  $E_{OCP}$  value to record the PDP curves. The Tafel region of the PDP curves were used to extrapolate all electrochemical parameters. At a scan rate of 0.125 mV/s, the mild steel surface was polarized by  $\pm 10$  mV against the  $E_{OCP}$  to record the LPR curves. Polarization resistance values ( $R_p$ ) were recorded by selecting two points on the LPR curves, keeping the zero current value roughly in the middle. The IEs values from the PDP and LPR techniques,  $\eta_{PDP}(\%)$  and  $\eta_{LPR}(\%)$ , respectively, were calculated using Eqs. (5) and (6).

$$\eta_{PDP}(\%) = \left(1 - \frac{i_{corr}}{i_{corr}^{\circ}}\right) \times 100 \quad (5)$$

$$\eta_{LPR}(\%) = \left(1 - \frac{R_p^{\circ}}{R_p}\right) \times 100 \quad (6)$$

Where,  $i_{corr}^{\circ}$  and  $i_{corr}$  denote corrosion current densities in the absence and presence of the inhibitor, respectively, and  $R_p^{\circ}$  and  $R_p$  represent polarization resistances in the absence and presence of the inhibitor, respectively.

## 2.5. Surface studies

Mild steel coupons with smaller dimensions (1 cm  $\times$  1 cm  $\times$  0.3 cm) were used for surface evaluation. The coupons were thoroughly abraded with SiC papers of different grit sizes (#120 – #1200), followed by rinsing with acetone to remove moisture and drying in warm air before carrying out the immersion tests. The concentration of inhibitor **3** used for surface analyses was 50 ppm. After completing the immersion tests, which continued for 3 h, the coupons were taken out, dried in a cold stream of air, and submitted for analysis. Scanning electron microscopy (SEM) analyses were carried out using Quattro ESEM – FEG (Thermo Fisher Scientific) coupled with an EDX (Oxford Instruments). X-ray photoelectron spectroscopy (XPS) studies that revealed the bound state of the adsorbed elements were carried out by a Thermo Fisher Scientific ESCALAB 250Xi XPS microprobe. The microprobe could produce monochromatic Al K $\alpha$  X-ray radiations with photon energy 1486.7 eV and wavelength 8.3386 Å. The spot size and base pressure were maintained at 650  $\mu$ m and  $10^{-10}$  mbar, respectively. Avantage (version: 5.51) software was used to deconvolute the XPS spectra and fit the peaks. Water contact angle measurements were carried out using the KRÜSS Drop Shape Analyzer (DSA30E). The volume of each drop was maintained at 2  $\mu$ L and formed at a rate of 2.67  $\mu$ L/s. The analysis was performed using the sessile drop orientation and ellipse fitting method.

## 2.6. Density functional theory

Density functional theory (DFT)-based quantum chemical calculations were performed using a very popular DFT functional called B3LYP. The calculations were performed using Gaussian 09, and the basis set selected for this purpose was 6-31G+(d,p) [20]. The electronic properties associated with the corrosion inhibitor dictate how good the inhibitor is [21]. Different reactivity parameters derived from the frontier molecular orbitals (FMOs) energies were calculated using Eqs. (7)–(13):

$$\Delta E = E_{LUMO} - E_{HOMO} \quad (7)$$

$$IP = -E_{HOMO} \quad (8)$$

$$EA = -E_{LUMO} \quad (9)$$

$$\eta = \frac{1}{2}(E_{LUMO} - E_{HOMO}) \quad (10)$$

$$\sigma = 1/\eta \quad (11)$$

$$\chi = -\frac{1}{2}(E_{LUMO} + E_{HOMO}) \quad (12)$$

$$\Delta N = \frac{\chi_{Fe} - \chi_{inh}}{2(\eta_{Fe} + \eta_{inh})} \quad (13)$$

Where,  $\Delta E$  stands for HOMO–LUMO gap,  $IP$  represents ionization potential, and  $EA$  means electron affinity. On the other hand,  $\eta$  and  $\sigma$  represent global hardness and global softness, respectively.  $\chi$  represents electronegativity, and  $\Delta N$  indicates the fraction of electron transfer.

### 3. Results and discussion

#### 3.1. Characterization of quaternary ammonium salt inhibitor (3)

The comprehensive elemental analysis of the inhibitor molecule **3**, with the molecular formula  $C_{28}H_{49}ClN_2$  (MW; 449.16  $g\ mol^{-1}$ ), FTIR,  $^1H$ , and  $^{13}C$  Nuclear magnetic resonance (NMR) spectra, and thermogravimetry analysis (TGA), is presented below.

The elemental analysis of inhibitor molecule **3**, with the molecular formula  $C_{28}H_{49}ClN_2$  (MW; 449.16  $g\ mol^{-1}$ ), found C 74.3, H 11.3, and N 5.9 %.  $C_{28}H_{49}ClN_2$  requires C 74.87; H 11.00; N 6.24 %.  $\nu_{max}$  (KBr): 3451 (moisture), 3077, 3008, 2922, 2853, 2808, 2708, 1842, 1642, 1617, 1514, 1485, 1468, 1418, 1368, 1258, 1220, 1149, 1119, 1074, 996, 919, 872, 818, 760, 722, 642, 561, and 465  $cm^{-1}$  (see supplementary information, Fig. S1).

$\delta H$  (CDCl<sub>3</sub>) 0.88 (3H, t, J 7.2 Hz), 1.10–1.35 (18 H, m), 1.72 (2H, m), 2.17 (moisture, br), 3.07 (4H, d, J 6.4 Hz) 3.31 (6H, s), 3.46 (2H, m), 3.59 (2H, s), 4.97 (2H, s), 5.17 (4H, m), 5.86 (2H, m), 7.43 (2H, d, J 7.8 Hz), 7.56 (2H, d, J 7.8 Hz);  $\delta C$  (CDCl<sub>3</sub>) 13.93 (1C), 22.47 (1C), 22.73 (1C), 26.13 (1C), 29.07 (1C), 29.11 (1C), 29.18 (1C), 29.24 (2C), 29.37 (1C), 31.69 (1C), 49.40 (2C), 56.36 (2C), 56.76 (1C), 63.19 (1C), 66.94 (1C), 117.45 (2C), 125.72 (1C), 129.13 (2C), 132.90 (2C), 135.33 (2C), 142.53 (1C). (CDCl<sub>3</sub> middle C:77.00).

The  $^1H$  and  $^{13}C$  NMR spectra of inhibitor molecule **3** with the relevant assignments are depicted in Fig. 1.

As shown in Fig. S2, the TGA curve depicts the thermal stability of the inhibitor molecule **3** is up to  $\approx 200^\circ C$ .

#### 3.2. Gravimetric studies

##### 3.2.1. Effect of concentration and temperature

To understand the effect of inhibitor **3** on the corrosion of mild steel in 15 % HCl, gravimetric WL studies were carried out for different concentrations of inhibitor **3** at 30 °C. Table 1 shows the extent of WL occurred in the absence and presence of 1, 5, 10, 20, 50, and 100 ppm of inhibitor **3**. In the absence of inhibitor **3**, highly corrosive 15 % HCl caused the mild steel coupon to experience a WL of

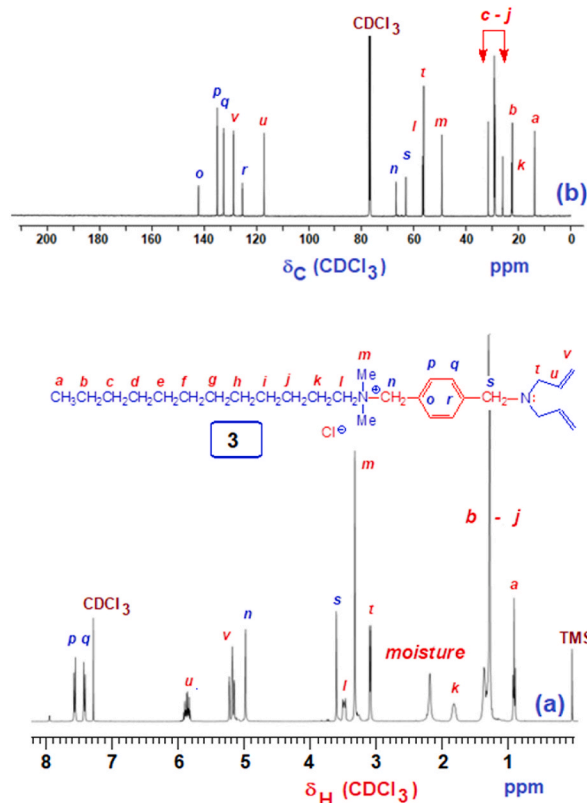


Fig. 1. (a)  $^1H$  and (b)  $^{13}C$  NMR spectrum of inhibitor molecule **3** in CDCl<sub>3</sub>.

**Table 1**Weight loss study data for the corrosion of mild steel in the presence and absence of inhibitor **3** in 15 % HCl at different temperatures.

Temp (°C)	Conc. (ppm)	Weight loss (mg) <sup>a</sup>	CR (mm y <sup>-1</sup> ) <sup>a</sup>	Surface coverage ( $\theta$ )	$\eta_{wl}$ (%) <sup>a</sup>
30	Blank	224.4 ± 0.70	33.7 ± 0.11	–	–
	1	215.2 ± 0.44	32.3 ± 0.07	0.041	4.1 ± 0.43
	5	105 ± 0.56	15.8 ± 0.08	0.532	53.2 ± 0.14
	10	51.4 ± 0.46	7.7 ± 0.07	0.771	77.1 ± 0.24
	20	26 ± 0.66	3.9 ± 0.10	0.884	88.4 ± 0.26
	50	13 ± 1.01	2 ± 0.15	0.942	94.2 ± 0.44
	100	12.3 ± 0.26	1.9 ± 0.04	0.945	94.5 ± 0.11
40	Blank	499.8 ± 0.26	75.1 ± 0.04	–	–
	50	43.3 ± 0.20	6.5 ± 0.03	0.913	91.3 ± 0.04
50	Blank	1099.1 ± 1.15	165.2 ± 0.17	–	–
	50	188.9 ± 0.96	28.4 ± 0.14	0.828	82.8 ± 0.10
60	Blank	2278.5 ± 0.46	342.4 ± 0.07	–	–
	50	568.6 ± 0.61	85.5 ± 0.09	0.750	75.0 ± 0.03

<sup>a</sup> The numerical values after ‘±’ represent the standard deviation.

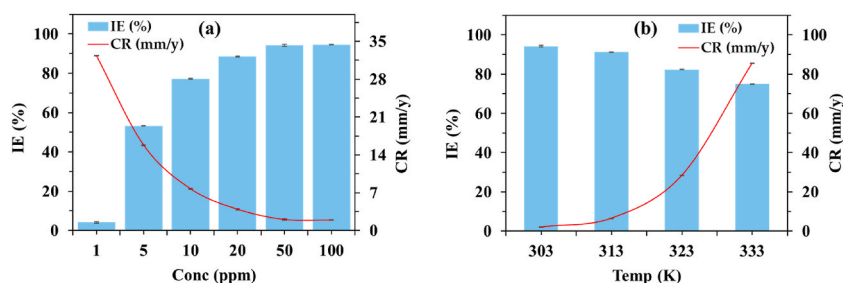
224.4 mg. The WL was found to be a little less following the immersion of mild steel in 1 ppm inhibitor **3** solution. However, CR values started declining significantly starting from the concentration of 5 ppm and onwards. Whereas 1 ppm of inhibitor **3** imparted a low IE of 4.1 %, it improved to 53.2 % in the presence of 5 ppm. After that, with increasing concentrations, the IE started increasing, and CR values kept declining. At 10, 20, 50, and 100 ppm of **3**, the IE values were calculated to be 77.1, 88.4, 94.2, and 94.5 %, respectively. In the absence of inhibitor **3**, CR was found to be 33.7 mm<sup>-1</sup>, which declined radically to 2 mm<sup>-1</sup> in the presence of 50 ppm of the inhibitor. Fig. 2a shows the variation in IE and CR values with the change in inhibitor concentration. A corrosion inhibitor is suitable for a specific electrolyte medium if the IE imparted by it is higher than 90 % at concentrations of tens or hundreds of ppm [22]. Inhibitor **3** reached a maximum IE of 94.2 % at only 50 ppm. The inhibitor molecule contains certain functionalities designed to help it adsorb better on the metal surface. The presence of a lone pair of electrons on nitrogen,  $\pi$ -electrons in the benzene ring, quaternary ammonium moiety, and chloride counter ions made physical and/or chemical interactions with the metal surface that are positively charged.

Additionally, an alkyl chain length in the inhibitor molecule certainly contributed to a surge in hydrophobicity on the metal surface that neutralized the aggression of corrosive water molecules [23]. However, the IE didn't experience any further increase after 50 ppm, as the IE values imparted by 50 and 100 ppm of inhibitor **3** are almost the same. This indicates that the adsorption sites on the metal surface are all occupied by the inhibitor molecules present at the concentration of 50 ppm. Therefore, increasing the concentration after that doesn't help anymore. Thus, 50 ppm of inhibitor **3** is the optimum concentration to achieve the best performance.

As inhibitor **3** showed the maximum IE at 50 ppm, this concentration was chosen for surface studies and observing the effect of temperatures that would reveal valuable thermodynamic parameters (vide infra, section 3.2.3). Table 1 and Fig. 2b show the variation in IE and CR values as mild steel coupons are tested in the presence and absence of 50 ppm of inhibitor **3** at different temperatures. At 40 °C, the IE was found to be 91.3 %, which is still very close to that obtained at 30 °C. At 50 °C and 60 °C, the IE values declined to 82.8 and 75.0 %, respectively. The IE of an inhibitor decreasing with increasing temperature can be linked to its adsorption via the physisorption/electrostatic interaction process, and this interaction gets weaker owing to thermal agitation [24]. Consequently, the CR values at 40, 50, and 60 °C were found to be 6.5, 28.4, and 85.5 mm<sup>-1</sup>, respectively, increasing from 2 mm<sup>-1</sup> at 30 °C.

### 3.2.2. Adsorption isotherm

The WL data obtained from corrosion of mild steel in the presence of **3** at 30 °C was used to fit several adsorption isotherms (Eq. (14) – (17)). Fig. S3 shows different adsorption isotherm curves, and Table 2 outlines the relevant isotherm parameters obtained from isotherm fittings. The Langmuir isotherm represents the best fit (Eq. (15)). The correlation of coefficient value ( $R^2$ ) for Langmuir adsorption isotherm was found to be the closest to unity, indicating a much better fitting than  $R^2$  values of 0.8073, 0.8953, and 0.7590



**Fig. 2.** Change in IE and CR values for mild steel corrosion in the presence of inhibitor **3** at 30 °C (a) and 50 ppm of **3** at different temperatures (b).

**Table 2**

Different isotherm parameters were obtained from WL studies carried out at 30 °C.

Temkin		Frumkin		Freundlich		Langmuir		
R <sup>2</sup>	f	R <sup>2</sup>	a	R <sup>2</sup>	n	R <sup>2</sup>	K <sub>ads</sub> (L mol <sup>-1</sup> )	ΔG <sub>ads</sub> <sup>o</sup> (kJ mol <sup>-1</sup> )
0.8073	7.741	0.8953	7.108	0.7590	0.1744	0.9994	1.53 × 10 <sup>5</sup>	-40.19

obtained for Temkin, Frumkin, and Freundlich adsorption isotherms, respectively. Fig. S3a shows that the slope value obtained for Langmuir isotherm fitting is 1.0228, which is very close to 1. This indicates that the adsorption of inhibitor 3 on a mild steel surface follows the monolayer adsorption model [25].  $K_{ads}$  was calculated from the intercept of Langmuir adsorption isotherm and was found to have a very large value of  $1.53 \times 10^5$  L mol<sup>-1</sup>, indicating a strong attractive force between inhibitor 3 and the metal surface. While the nature of Gibbs free energy value ( $\Delta G_{ads}^o$ ) discloses the spontaneity of the adsorption process; its magnitude reveals the type of adsorption process adopted by the inhibitor.  $\Delta G_{ads}^o$  value for Langmuir adsorption isotherm was calculated following Eq. (18) and found to be  $-40.19$  kJ mol<sup>-1</sup>, as enumerated in Table 2. The negative value of  $\Delta G_{ads}^o$  proves that the adsorption of 3 on a mild steel surface is spontaneous. Generally, while  $\Delta G_{ads}^o$  value of  $-20$  kJ mol<sup>-1</sup> or less negative indicates an electrostatic interaction between the inhibitor and the metal surface, and a value of  $-40$  kJ mol<sup>-1</sup> or more negative suggests that electrons transfer the inhibitor to the metal surface [26]. Therefore, the calculated  $\Delta G_{ads}^o$  value of  $-40.19$  kJ mol<sup>-1</sup> for the adsorption of inhibitor 3 suggests a mixed interplay between these two adsorption modes.

$$\text{Freundlich : } \log \theta = n \log C + \log K_{ads} \quad (14)$$

$$\text{Langmuir : } C/\theta = C + 1/K_{ads} \quad (15)$$

$$\text{Fumkin : } \theta = \frac{2.303}{2a} \log \frac{\theta}{(1-\theta)C} - \frac{2.303}{2a} \log K_{ads} \quad (16)$$

$$\text{Temkin : } \theta = \frac{2.303}{f} \log C - \frac{2.303}{f} \log K_{ads} \quad (17)$$

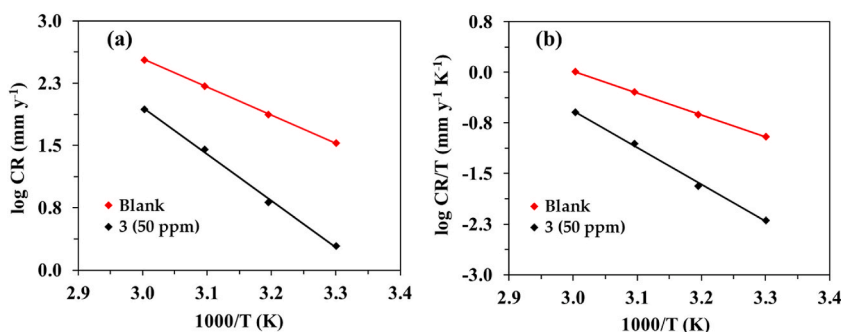
$$\Delta G_{ads}^o = -RT \ln (55.5 \times K_{ads}) \quad (18)$$

Where,  $\theta$  represents surface coverage,  $C$  indicates inhibitor concentration (M),  $K_{ads}$  is the adsorption constant,  $n$ ,  $a$ , and  $f$  are Freundlich, Frumkin, and Temkin adsorbate characteristics, respectively. In Eq. (18),  $\Delta G_{ads}^o$  is the thermodynamic potential popularly known as Gibbs free energy,  $R$  is the universal gas constant having a value of  $8.314$  J mol<sup>-1</sup> K<sup>-1</sup>, and  $T$  represents the absolute temperature in Kelvin, and  $55.5$  is the moles of water in 1 L of water.

### 3.2.3. Thermodynamic parameters

The study on the effect of temperature on CR (vide supra; section 3.2.1) was used to estimate the thermodynamic parameters, such as activation energy ( $E_a$ ), enthalpy ( $\Delta H_{ads}$ ), and entropy ( $\Delta S_{ads}$ ) of adsorption. The slope of the plot  $\log CR$  vs  $1/T(K)$  was used to estimate  $E_a$  following Eq. (19) (Arrhenius equation). On the other hand,  $\Delta H_{ads}$  and  $\Delta S_{ads}$  were obtained from the slope and intercept, respectively, of the plot  $\log CR/T$  vs.  $1/T(K)$  following Eq. (20) (transition state equation).

$$\log CR = \log A - \frac{E_a}{2.303RT} \quad (19)$$



**Fig. 3.**  $\log CR$  vs  $1/T(K)$  (Arrhenius plot) (a) to calculate the  $E_a$  value and  $\log CR/T$  vs.  $1/T(K)$  (transition state plot) (b) providing  $\Delta S_{ads}$  and  $\Delta H_{ads}$  parameters for iron dissolution in the absence and presence of inhibitor 3 (50 ppm) at different temperatures (303–333 K).

$$\log CR/T = \left[ \log \left( \frac{R}{Nh} \right) + \left( \frac{\Delta S_{ads}}{2.303R} \right) \right] - \frac{\Delta H_{ads}}{2.303RT} \quad (20)$$

Where,  $A$  is the Arrhenius pre-exponential factor,  $R$  is the molar gas constant,  $N$  is Avogadro's constant, and  $h$  represents Planck's constant.

Arrhenius and transition state plots are represented by Fig. 3a and b, respectively. Several important thermodynamic parameters were obtained using these two plots. While the  $E_a$  value for the blank solution was calculated to be  $65 \text{ kJ mol}^{-1}$ , the  $E_a$  value for 50 ppm-inhibited solution turned to be  $107.4 \text{ kJ mol}^{-1}$ . The rise in the  $E_a$  value in the presence of inhibitor **3** indicates that the dissolution of the metal has become more difficult [27,28]. In the absence and presence of inhibitor **3**, the values of  $\Delta H_{ads}$  were calculated to be  $62.3$  and  $104.8 \text{ kJ mol}^{-1}$ , respectively. This means the adsorption of inhibitor **3** is endothermic in nature, and the mild steel dissolution lessens in the presence of the inhibitor [25]. The value of  $\Delta S_{ads}$ , in the absence of inhibitor **3**, was found to be  $-10.3 \text{ J mol}^{-1} \text{ K}^{-1}$ . An increase in  $\Delta S_{ads}$  from  $-10.3 \text{ J mol}^{-1} \text{ K}^{-1}$  to a very high value of  $106.1 \text{ J mol}^{-1} \text{ K}^{-1}$  for the inhibitor adsorption indicates an increase in the disorder on the mild steel surface. This could be attributed to a faster displacement of the water molecules from the mild steel surface while the inhibitor molecules are adsorbed, providing better protection [29].

### 3.3. Electrochemical corrosion studies

#### 3.3.1. Open circuit potential (OCP)

Fig. 4a shows the potential-time curves (OCP curves) that were recorded after allowing the mild steel to corrode freely for 1 h at  $30^\circ \text{C}$  in the absence and presence of different concentrations of inhibitor **3**. These OCP curves show how, both in the presence and absence of the inhibitor, the electrical double layer on the metal surface adapts to the corrosive environment. The  $E_{OCP}$  of the blank is shown to begin at around  $-510 \text{ mV vs. SCE}$  and continues progressing in the anodic/(+ve) direction until a steady state is reached. This behavior can be explained as an attempt by the metal surface to develop a protective oxide layer following the corrosive attack of 15 % HCl solution [30]. An identical response could be observed when various amounts of inhibitor **3** are added to the harsh 15 % HCl solution. In the presence of 1, 5, 10, 20, 50, and 100 ppm of inhibitor **3**,  $E_{OCP}$  starts moving towards the (+ve) direction as the curve progresses. This suggests that inhibitor **3** functions by inspiring an anodic direction inhibition mechanism. However, since none of the  $E_{OCP}$  shifts corresponding to different concentrations of **3** experienced a drift of more than 85 mV from that of the blank solution, the inhibition mechanism can be assumed to be of mixed-type, i.e., inhibitor **3** functions by retarding both anodic and cathodic half-cell

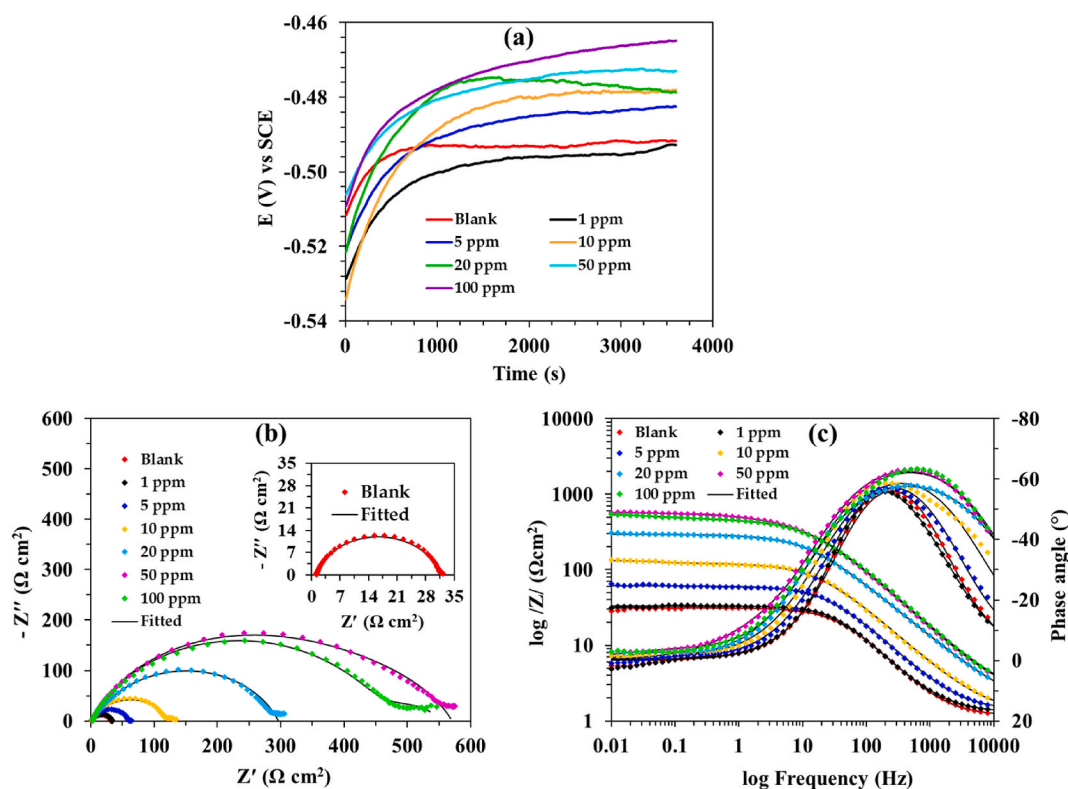


Fig. 4. OCP curves recorded for the corrosion of mild steel in the absence and presence of different concentrations of **3** in 15 % HCl for 1 h at  $30^\circ \text{C}$  (a); EIS-mediated Nyquist plots (b) and Bode magnitude (along primary vertical axis) and phase angle (along secondary vertical axis) plots (c) recorded under the same conditions as OCP curves.



reactions [31,32]. Importantly, as each OCP curve was observed to attain a steady state within 1 h, electrochemical measurements were able to be conducted under a stable system free of potential drift.

### 3.3.2. Electrochemical impedance spectroscopy (EIS)

The nature of the newly constructed electrical double layer (EDL) following OCP stabilization was evaluated in terms of EIS measurements represented by Nyquist plot (Fig. 4b), Bode magnitude (along the primary vertical axis), and Bode phase angle (along the secondary vertical axis) plots (Fig. 4c) in 15 % HCl with varying inhibitor 3 doses present and absent. In the control 15 % HCl solution, the Nyquist plot (Fig. 4b inset) represents a depressed semicircle with solution ( $R_s$ ) and charge transfer ( $R_{ct}$ ) resistances of 1.18 and 30.27  $\Omega\text{cm}^2$ , respectively. In a blank solution, the Nyquist plot is characterized by a single capacitive loop, a trait ascribed to characteristics of a solid electrode surface showing a charge transfer controlled mechanism in a corrosive medium [12,33]. The diameter of the depressed semicircles increased for 1, 5, 10, 20, 50, and 100 ppm of inhibitor 3 with that of blank 15 % HCl. This indicates the adsorption of inhibitor 3 on the metal surface by removing the corrosive species, including water molecules. However, the semicircle corresponding to 100 ppm of inhibitor 3 turned out to be smaller than that of 50 ppm. This can be attributed to introducing a 50 ppm inhibitor solution to the corrosive medium that thoroughly covers the mild steel surface. Increasing the inhibitor concentration further doesn't increase adsorption and can cause the desorption of inhibitor molecules that have already been adsorbed [34,35]. Fig. 4c depicts the Bode magnitude and phase angle plots that further confirm the concentration dependency of inhibitor 3, as already evidenced by Nyquist plots [36,37]. In Fig. 4c, the logarithm of modulus impedance ( $\log |Z|$ ) increases proportionately with increasing inhibitor concentration, reaching a maximum value at an inhibitor concentration of 50 ppm.

In Fig. 4c, the phase angle plots responsible for different concentrations of inhibitor 3 are characterized by broad deflection points with respect to that of blank in the high-frequency region. This can be explained by the fact that the electrochemical fitting of neither the Nyquist plots nor the Bode magnitude plots showed the presence of more than one capacitive loop. The adsorbing inhibitor molecules shield the metal surface against HCl attack and might influence the occurrence of a second loop that Bode phase angle graphs show. When inhibitor 3 is not present, the capacitive loop can be explained by a single, one-time constant that represents a single relaxation process. However, the capacitive loops with inhibitor 3, indicating at least two time constants, imply that multiple relaxation processes occur at the surface [38,39]. The phase angle readings were found to be all below  $90^\circ$  in both the presence and absence of inhibitor 3 at various doses. During the relaxation process, a smaller deflection angle ( $<90^\circ$ ) can be linked to the surface roughness and inhomogeneity of dielectric materials. However, it is clear that the values of phase angle increase with increasing inhibitor concentrations, which signifies more inhibitive performance due to inhibitor adsorption [40,41]. Fig. 5a and b, respectively, show the equivalent circuits used to fit the EIS plots in the absence and presence of inhibitor 3. Equivalent circuits with one (Fig. 5a) and two (Fig. 5b) time constants were adopted to fit EIS plots corresponding to control 15 % HCl and inhibited solutions, respectively. Because of a rough and porous surface that deviates from the optimum behavior of a capacitor, EDL ( $Y_{dl}$ ) and the protective film ( $Y_{fm}$ ) generated on the mild steel surface as a result of the adsorption of 3 are incorporated into the expression for the CPE impedance function (Eq. (21)). The exponential value  $n$  ( $n_{dl}$  and  $n_{fm}$  for the EDL and protective film, respectively) that determines the electrical behavior is also included in Eq. (21). The EDL can be considered an ideal capacitor if the electrical behavior caused by surface inhomogeneity causes the  $n$  value to equate to 1 [42].

$$Z_{CPE} = Y_o^{-1} (j\omega)^{-n} \quad (21)$$

Where,  $Y_o$  represents the capacitive constant,  $\omega$  is the radial frequency, and  $j$  is an imaginary number used to resolve impedance and reactance from pure resistance.

The relevant impedance parameters are generated by fitting the impedance data in the absence and presence of inhibitor 3 using the circuits depicted in Fig. 5a and b are enumerated in Table 3. The chi-squared ( $\chi^2$ ) values were found to be  $< 0.001$ , indicating that the impedance plots were fitted very well. Almost all of the measured values of  $n_{dl}$  and  $n_{fm}$  varies in the range of 0.5–1, indicating the presence of a non-ideal capacitor in a charge transfer corrosion process [43,44].  $C_{dl}$  values were calculated using Eq. (22) and were found to decrease with increasing concentrations. While the  $C_{dl}$  value for the uninhibited solution was found to be 80.69  $\mu\text{F}/\text{cm}^2$ ; it decreased to 59.58, 42.62, 18.37, 8.29, 3.51, and 5.15  $\mu\text{F}/\text{cm}^2$  for 1, 5, 10, 20, 50, and 100 ppm solutions, respectively, of inhibitor 3. As more inhibitors adsorb on the metal surface and the thickness of the double layer increases, the  $C_{dl}$  values decrease accordingly (Eq. (23)).

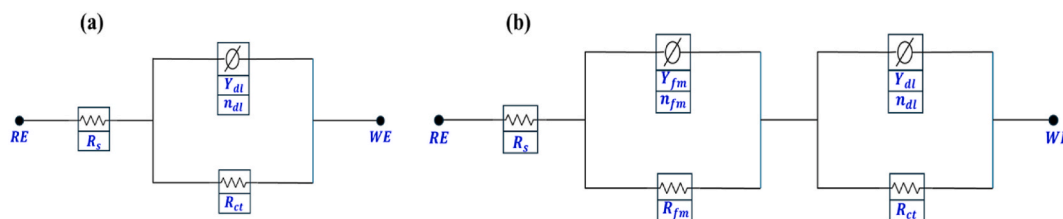


Fig. 5. Equivalent circuits for mild steel corrosion in 15 % HCl were utilized to fit the EIS data obtained in the absence (a) and presence (b) of inhibitor 3.

**Table 3**

The parameters of electrochemical impedance were acquired by fitting the Nyquist and Bode plots that were recorded for mild steel corrosion at 30 °C in 15 % HCl with and without inhibitor 3.

Conc. (ppm)	$R_s$ ( $\Omega\text{cm}^2$ )	$CPE_{fm}$			$CPE_{dl}$				$R_T$ ( $\Omega\text{cm}^2$ )	$\eta_{EIS}$ (%)	$\chi^2 \times 10^{-3}$
		$Y_{fm}$ ( $\mu\text{Scm}^2$ )	$n_{fm}$	$R_{fm}$ ( $\Omega\text{cm}^2$ )	$Y_{dl}$ ( $\mu\text{Scm}^2$ )	$n_{dl}$	$R_{ct}$ ( $\Omega\text{cm}^2$ )	$C_{dl}$ ( $\mu\text{F}/\text{cm}^2$ )			
Blank	1.18	–	–	–	327.1	0.85	30.27	80.69	30.27	–	0.75
1	1.29	3438	0.73	0.70	280.5	0.89	31.02	59.58	31.72	4.60	0.35
5	1.38	20660	1.00	0.28	278	0.81	59.75	42.62	60.03	49.6	0.64
10	1.30	332600	1.00	10.16	212.8	0.77	121.8	18.37	131.96	77.1	1.58
20	1.56	1294	0.64	7.72	117.9	0.76	286.8	8.29	294.52	89.7	0.47
50	2.09	74.36	0.78	388.80	110.8	0.71	180.1	3.51	568.90	94.7	0.32
100	2.08	30.89	0.80	390.10	120.3	0.62	110.57	5.15	500.67	94.0	0.48

$$C_{dl} = Y_{dl} / n_{dl} \left( \frac{1}{R_s} + \frac{1}{R_{ct}} \right)^{(n_{dl} - 1)} / n_{dl} \quad (22)$$

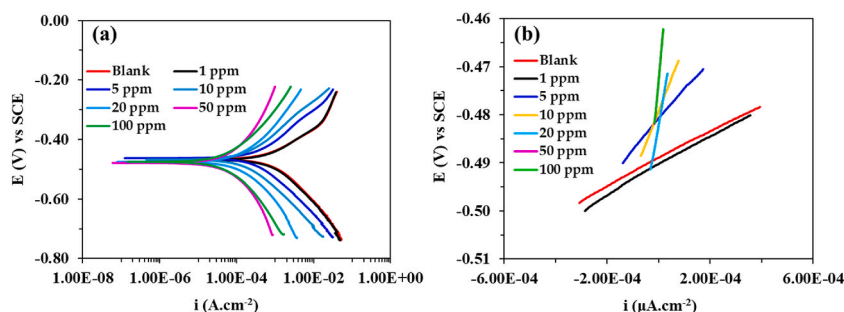
$$C_{dl} = \frac{\epsilon_0 \epsilon A}{d} \quad (23)$$

Where,  $C_{dl}$ ,  $R_s$ ,  $R_{ct}$ , and  $n_{dl}$  represent the double-layer capacitance, solution resistance, charge-transfer resistance, and surface inhomogeneity, respectively, and  $A$ ,  $d$ ,  $\epsilon_0$ , and  $\epsilon$  denote the exposed metal surface area, EDL thickness, permittivity of air, and relative permittivity, respectively.

The  $R_{ct}$  values were also found to be increasing in relation to blank with increasing inhibitor concentrations. This indicates that the transfer/movement of  $\text{Fe}^{2+}/\text{Fe}^{3+}$  and other corrosive species across the EDL becomes increasingly difficult with additional film formation [45,46]. The adsorption of inhibitor 3 on the metal surface is strongly supported by the rise in  $R_{ct}$  values and decrease in  $C_{dl}$  values. This also testifies to the dependency of the IE on the concentration of the inhibitor until a certain dosage. As such, the IEs from the EIS technique were found to be 4.6, 49.6, 77.1, 89.7, 94.7, and 94.0 % for 1, 5, 10, 20, 50, and 100 ppm, respectively, of inhibitor adsorption.

### 3.3.3. Polarization measurements

Fig. 6a and b, respectively, show polarization measurements obtained at 303 K using linear polarization resistance (LPR) and potentiodynamic polarization (PDP) techniques. It showed that the extent of current density increased after the cathodic and anodic areas experienced a rise in the applied potential. Fig. 6a illustrates that an activation-controlled mechanism is in play for the metal corrosion in the studied acidizing solution. A number of significant electrochemical parameters were obtained by fitting the Tafel curves' cathodic and anodic lines, listed in Table 4. These electrochemical characteristics include the corrosion potential ( $E_{corr}$ ), the corrosion current density ( $i_{corr}$ ), the anodic ( $\beta_a$ ) and cathodic ( $\beta_c$ ) Tafel slopes, etc. The  $E_{corr}$  of the blank solution was found to be  $-466$  mV vs. SCE, which is still very close to that of  $-510$  mV for the blank recorded during OCP curves analysis.  $E_{corr}$  values recorded for different inhibited solutions in the presence of inhibitor 3 were also close to those found during OCP curves recording. This demonstrates that during the PDP measurements, there was minimal potential drift. Furthermore, none of the inhibited solutions'  $E_{corr}$  values differed from the blank by more than 85 mV. As previously found during the investigation of OCP curves, this suggests that inhibitor 3 is a mixed-type inhibitor that affects both half-cell reactions. This means that the adsorption of inhibitor 3 reduces the metal's anodic dissolution rates and the cathodic evolution of molecular hydrogen to more or less the same extent. Additionally, the reduction of the corrosion rate without the  $E_{corr}$  values being significantly altered implies the pickling-type behavior of inhibitor 3 [47–50]. The  $\beta_a$  and  $\beta_c$  values for the blank solution changed from 99.9 to 127 mV  $\text{dec}^{-1}$  to 97.7 and 128 mV  $\text{dec}^{-1}$ , respectively, for 1 ppm of inhibitor 3. The deviations were significantly more noticeable when inhibitor 3 concentration rose. This again reveals that the adsorption of inhibitor 3 on the metal surface affects both the cathodic and anodic processes. However, when the polarization potential



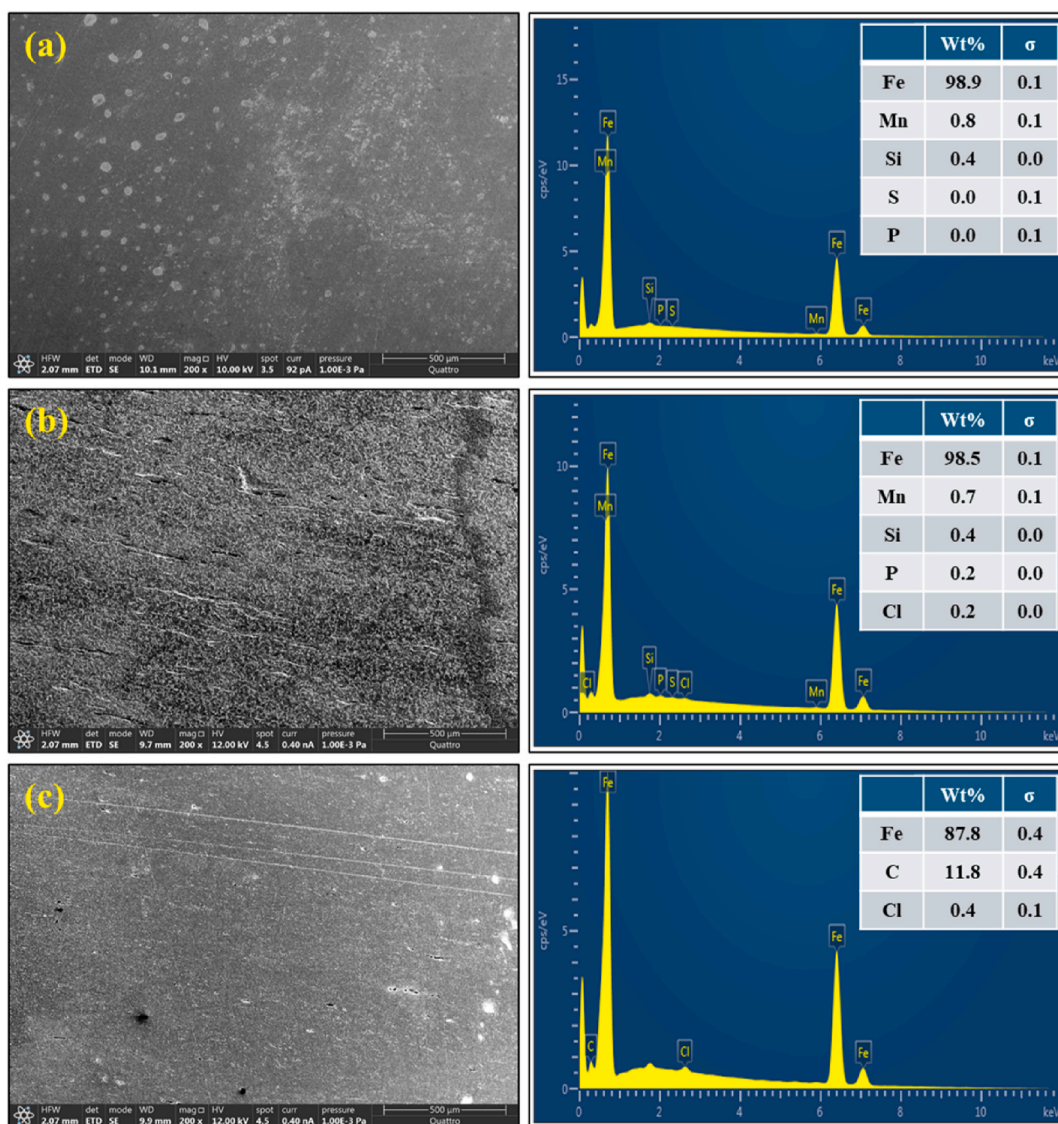
**Fig. 6.** Tafel curves (a) and linear polarization lines (b) following polarization measurements conducted in blank and inhibited solutions.

**Table 4**

PDP and LPR electrochemical parameters following the fitting of polarization curves recorded in both blank and inhibited solutions.

Conc. (ppm)			PDP			LPR	
	$E_{corr}$ (mV)	$\beta_a$ (mV dec <sup>-1</sup> )	$-\beta_c$ (mV dec <sup>-1</sup> )	$i_{corr}$ ( $\mu\text{A}\cdot\text{cm}^{-2}$ )	$\eta_{PDP}$ (%)	$R_p$ ( $\Omega\text{cm}^2$ )	$\eta_{LPR}$ (%)
Blank	-466	99.9	127	803	-	28.5	-
1	-468	97.7	128	766	4.6	29.9	4.7
5	-462	112	125	331	58.8	63.6	55.2
10	-468	113	120	170	78.8	138	79.3
20	-475	139	146	120	85.1	311	90.8
50	-479	164	157	64.9	91.9	600	95.2
100	-476	128	140	51.9	93.5	575	95.0

varies during PDP measurements, the disproportionate fluctuations in  $\beta_a$  and  $\beta_c$  values can be explained by the various degrees of mild steel surface roughness. When inhibitor **3** is not present, the  $i_{corr}$  value is  $803 \mu\text{A}\cdot\text{cm}^{-2}$ . In presence of 1, 5, 10, 20, 50, and 100 ppm of **3**,  $i_{corr}$  values reduced to 766, 331, 170, 120, 64.9, and  $51.9 \mu\text{A}\cdot\text{cm}^{-2}$ , respectively. This demonstrates that adding an inhibitor to a corrosive 15 % HCl reduces the corrosion rate significantly, and this effect is the most prominent for 50 ppm of inhibitor **3**. Therefore, the IE values, calculated following Eq. (5), corresponding to different concentrations of inhibitor **3** increase as the  $i_{corr}$  values decrease

**Fig. 7.** SEM micrographs (left) and EDX spectra (right) of clean (a), corroded (b), and inhibitor **3**-protected (c) metal surfaces.

in the series.

Fig. 6b shows that when the concentration of **3** in the solution rises, the LPR lines progressively tilt toward zero current. Therefore, with increasing concentration of **3**, mild steel surface experiences better protection. The IE values from LPR measurements were calculated following Eq. (6) after estimating the LPR line slopes as  $R_p$ . The values of  $R_p$  and  $\eta_{LPR}(\%)$  are enumerated in Table 4. In the absence of inhibitor **3**, the  $R_p$  was recorded to be  $28.5 \Omega\text{cm}^2$ . The  $R_p$  values kept increasing with increasing inhibitor concentration. From  $28.5 \Omega\text{cm}^2$  for blank, the  $R_p$  values increased to 29.9, 63.6, 138, 311, 600, and  $575 \Omega\text{cm}^2$  in the presence of 1, 5, 10, 20, 50, and 100 ppm of inhibitor **3**. Consequently, the IE values kept rising as well. In presence of 1, 5, 10, 20, 50, and 100 ppm of **3**,  $\eta_{LPR}(\%)$  values were calculated as 4.70, 55.2, 79.3, 90.8, 95.2, and 95.0 %, respectively. PDP and LPR procedures produced IE values consistent with WL and EIS techniques.

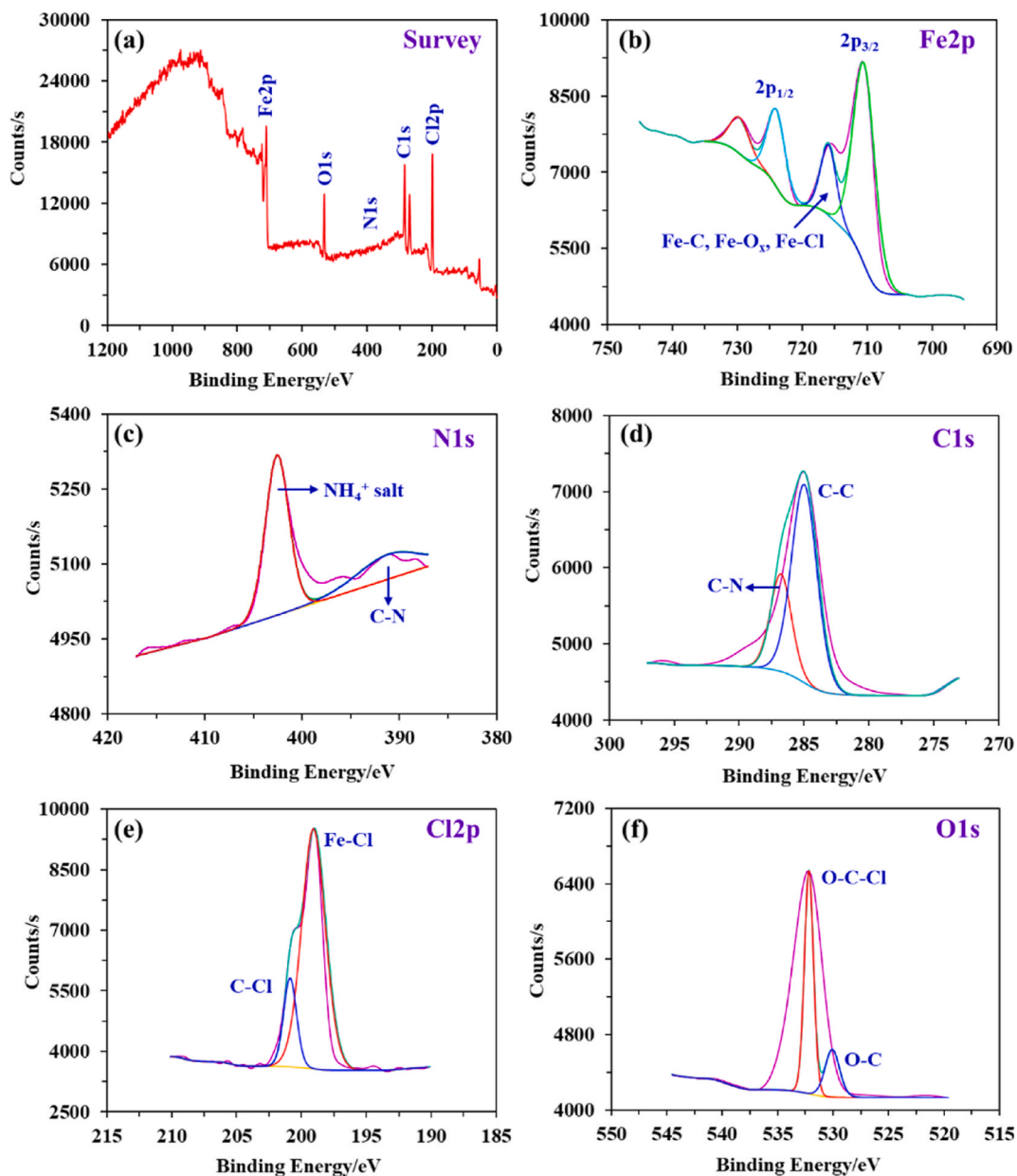


Fig. 8. XPS survey (a) and deconvoluted XPS spectra of Fe2p (b), N1s (c), Cl1s (d), Cl2p (e), and O1s (f) for mild steel immersed in 15 % HCl in the presence of 50 ppm inhibitor **3** at 30 °C.

### 3.4. Surface studies

#### 3.4.1. SEM-EDX

After completely submerging in the examined electrolyte at 303 K with and without 50 ppm inhibitor **3**, the surface appearance and constituent compositions of the metal coupons were examined, as shown in Fig. 7. The surface appearance and elemental composition of a polished, clean, mild steel surface are shown in Fig. 7a. The surface looks nice and smooth without any sign of roughness or cracks. EDX analysis showed the presence of Fe (98.9 %) and other atoms relevant to mild steel. Fig. 7b shows the surface morphology and EDX spectrum of the mild steel surface treated in 15 % HCl without any inhibitor. The surface looks very uneven and rough, with multiple sights showing the attack of  $\text{Cl}^-$  ions. In the absence of any inhibitor, the mild steel surface wasn't offered any protection and was corroded severely. This caused a slight reduction in the elemental composition of Fe (98.5 %) and showed the presence of an additional Cl peak (0.2 %). Fig. 7c depicts the surface morphology and EDX spectra of a mild steel surface treated in 15 % HCl with 50 ppm inhibitor **3**. Compared to the surface shown in Fig. 7b, the inhibitor-protected surface in Fig. 7c is much smoother, with one or two sights of aggressiveness from the  $\text{Cl}^-$  ions. The EDX spectrum shows a peak for the presence of C (11.8 %), which originated from the adsorption of inhibitor **3**. Interestingly, the wt.% of the Cl peak increased from 0.2 % for the corroded surface to 0.4 % for the inhibited surface owing to the presence of  $\text{Cl}^-$  counter ions present in the inhibitor molecules. Therefore, the existence of a reasonably extended hydrophobic alkyl chain length, a positively charged quaternary ammonium moiety,  $\pi$ -electrons, and unquenched electrons on nitrogen in the diallylamine moiety have all helped inhibitor **3** to act as an excellent corrosion inhibitor.

#### 3.4.2. XPS

XPS survey spectrum and the deconvoluted spectra for Fe2p, N1s, C1s, O1s, and Cl2p, achieved following XPS experiments and software fittings, are shown in Fig. 8. In the survey spectrum (Fig. 8a), Fe2p, O1s, C1s, and Cl2p are very clearly visible along with some other peaks relevant to mild steel. However, the peak for N1s is barely noticeable because nitrogen's contribution to the overall composition of inhibitor **3** is minimal, and only a small amount of inhibitor **3** is present in the corrosive medium. The deconvoluted Fe2p spectrum (Fig. 8b) shows two spin orbitals ( $2p_{1/2}$  and  $2p_{3/2}$ ) comprising both  $\text{Fe}^{2+}$  and  $\text{Fe}^{3+}$  without satellite peaks [51,52]. The percentage composition of Fe (II) and Fe(III) species that are anticipated to form various chlorides, oxides, carbides, and hydroxides [53] are 75.69 and 24.31 %, respectively (Table 5). In Fig. 8c, the presence of two peaks at 402.58 (74.4 %) and 391.48 eV (25.6 %) can be correlated with  $\text{NH}_4^+$  salt and C–N, respectively [53–55]. These two peaks' existence in the deconvoluted spectra of N1s indicates that the inhibitor adheres to the metal surface. In C1s deconvoluted spectrum (Fig. 8d), the presence of a high atomic wt% (70.75 %) peak at 284.88 eV and relatively lower atomic wt% (29.25 %) at 286.68 eV are ascribed to C–C and C–N, respectively [56,57], owing to mild steel surface accommodating the long alkyl hydrophobic chain and nitrogen atoms from inhibitor **3**. The presence of a high atomic wt% (83.08 %) peak at 198.88 eV in the Cl2p deconvoluted spectrum (Fig. 8e) can be traced to the presence of  $\text{FeCl}_2$  and  $\text{FeCl}_3$  species (Fe–Cl) on the metal surface [25]. An additional peak at more than 200 eV from organic chloride (C–Cl) arises from the interaction between inhibitor **3** and  $\text{Cl}^-$  ions. The deconvoluted O1s spectrum (Fig. 8f) shows a very dominant peak at 532.18 eV and another relatively smaller peak at 530.8 eV owing to O–C–Cl and O–C, respectively [58,59]. These peaks confirm the interactions among oxygen, inhibitor **3**, and the  $\text{Cl}^-$  ions present in the corrosive environment. Overall, the detailed analyses based on the interpretation of the presented deconvoluted spectra can be used to establish efficient adsorption of inhibitor **3** on the metal surface.

#### 3.4.3. Contact angle measurements

The recorded water contact angle values ( $\theta_{\text{H}_2\text{O}}$ ) of the polished, corroded, and inhibited mild steel surfaces are shown in Fig. 9. It has been reported that a surface can be susceptible to wetting if its  $\theta_{\text{H}_2\text{O}}$  is lesser than  $90^\circ$  and water-repellent if  $\theta_{\text{H}_2\text{O}}$  is greater than  $90^\circ$  [60]. The polished surface (Fig. 9a) shows a  $\theta_{\text{H}_2\text{O}}$  value of  $89.1^\circ$  indicates that a bare, unexposed surface is considerably hydrophobic. However, when the same surface was exposed to corrosive 15 % HCl at  $30^\circ\text{C}$ , the  $\theta_{\text{H}_2\text{O}}$  value reduced to a very low  $20.4^\circ$  (Fig. 9b). After severe corrosion in 15 % HCl, the surface's hydrophobic nature degrades, and wettability increases. Fig. 9c shows the surface and  $\theta_{\text{H}_2\text{O}}$  value for a mild steel surface treated in 50 ppm of inhibitor **3**. The  $\theta_{\text{H}_2\text{O}}$  value for the inhibited surface increased to  $98.7^\circ$  from  $20.4^\circ$  for

**Table 5**

Different XPS binding energy (BE) peaks and their relative amounts (%) are assigned to several species.

Element	Peak BE (eV)	Chemical state	Atomic %
Fe2p	710.48	$\text{Fe}^{2+}$ ( $2p_{3/2}$ )	57.11
	715.98	$\text{Fe}^{3+}$ ( $2p_{1/2}$ )	14.58
	723.98	$\text{Fe}^{2+}$ ( $2p_{3/2}$ )	18.58
	729.68	$\text{Fe}^{3+}$ ( $2p_{1/2}$ )	9.73
C1s	284.88	C–C	70.75
	286.68	C–N	29.25
N1s	402.58	$\text{NH}_4^+$ salt	74.4
	391.48	C–N	25.6
Cl2p	198.88	Fe–Cl	83.08
	200.78	C–Cl	16.92
O1s	532.18	O–C–Cl	74.64
	530.08	O–C	25.36

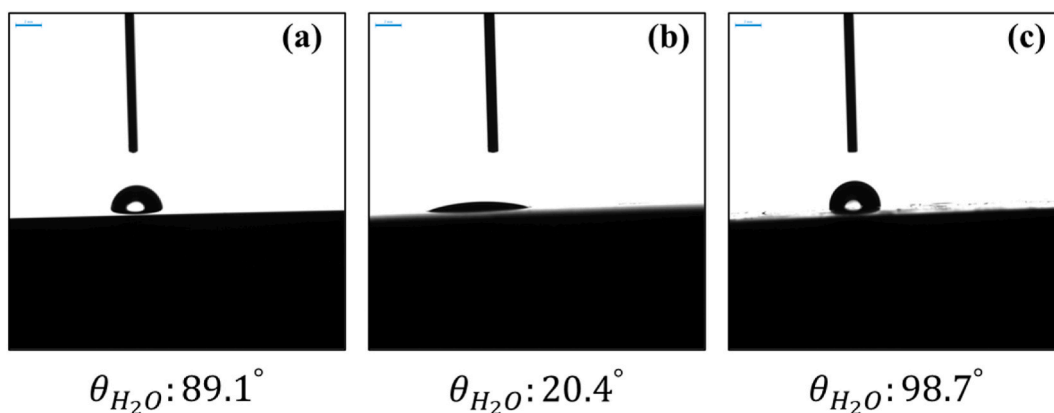


Fig. 9. The surfaces of polished (a), corroded (b), and inhibited (c) mild steel coupons show water contact angle values.

the corroded one. This demonstrates the inhibitor's efficacy in creating a hydrophobic barrier on the mild steel surface. This hydrophobic barrier limits the contact of water molecules and other aggressive corrosive ions with the metal surface.

### 3.5. Density functional theory calculations

The DFT-optimized structure and the frontier orbitals of inhibitor **3** are depicted in Fig. 10. Different theoretical parameters derived from the calculations are outlined in Table 6. It has been observed from Fig. 10 that the HOMO and LUMO regions are consolidated over the chloride counter ions and the quaternary ammonium and aromatic ring moieties, respectively. The inhibitor's HOMO and LUMO orbitals interact with the metal surface via electron donation and acceptance, respectively [61]. Therefore, it's evident that the chloride counter ions, the quaternary ammonium moiety, and the aromatic ring are crucial to the success of the inhibitor in mitigating mild steel corrosion in 15 % HCl. With an increase in  $E_{HOMO}$ , therefore, decrease in  $\Delta E$ , the ability of the inhibitor molecules to form bonds with the metal surface has been reported to increase [62]. While a low value of  $\Delta E$  is desired for better efficiency, inhibitor **3** having a HOMO-LUMO energy gap of 7.784 eV indicates a relatively easier movement of electrons from the inhibitor to the surface. The ionization energy ( $IE$ ) parameter is directly related to  $E_{HOMO}$ . The low lying  $IE$  value of only 5.865 eV indicates that it's relatively easier for inhibitor **3** to be ionized and donate electrons to the metal surface. On the other hand, a very low value of  $-1.973$  eV for electronegativity ( $\chi$ ) indicates that the inhibitor is more prone to donate electrons to the metal surface to promote surface coverage, as the first ionization energy of iron is  $\sim 8$  eV. The calculation of the hardness ( $\eta$ ) and softness ( $\sigma$ ) values are very important, as they reveal the efficacy of anticorrosion compounds. Usually, low hardness ( $\eta$ ) and high softness ( $\sigma$ ) values are desirable. The electrophilicity ( $\omega$ ) parameter also plays a vital role in dictating how efficient a corrosion inhibitor is. This parameter expresses the propensity of inhibitor molecules to receive electrons from the metal surface through retro-donation/backdonation [63]. A relatively high value of 7.578 eV for the electrophilicity parameter suggests that the inhibitor interacts strongly with the metal surface via retro-donation. If the fraction of electrons transferred,  $\Delta N$ , is less than zero ( $\Delta N < 0$ ), the electrons are moving from the metal surface to the inhibitor. On the other hand, if  $\Delta N > 0$ , it indicates that the electrons are moving from the inhibitor to the metal surface [64]. The latter ( $\Delta N > 0$ ) is the preferred situation for the interaction of inhibitor **3** with the mild steel surface. The dipole moment ( $\mu$ ) metric indicates a molecule's overall polarity or separation between negative and positive charges. Higher  $\mu$  values result in stronger adsorption of the inhibitor molecule onto the mild steel surface due to intramolecular interactions [65]. A very high value of 26.37 D has been observed for inhibitor **3**, indicating its strong adsorption on the metal surface.

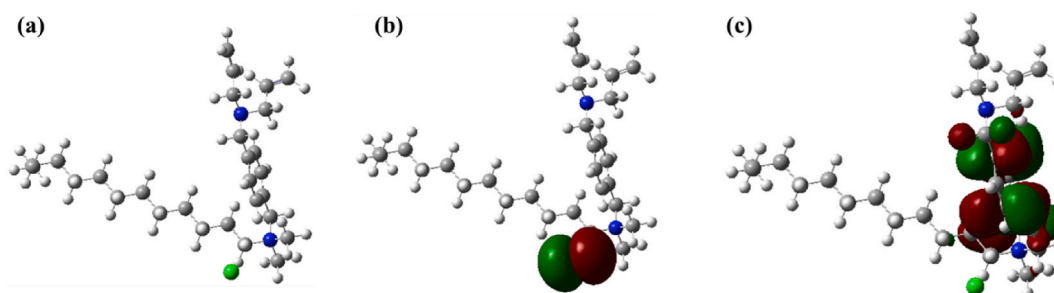
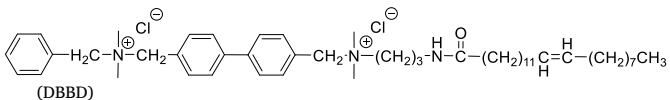
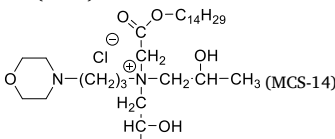
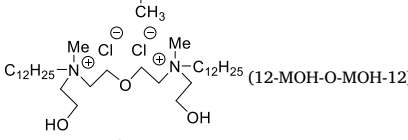
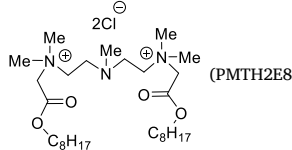
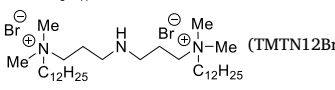
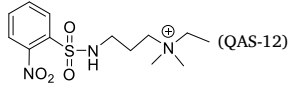
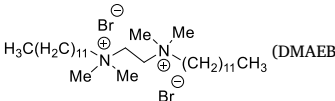
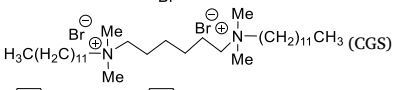

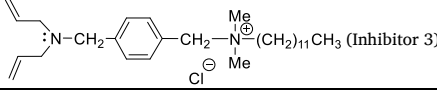


Fig. 10. Optimized structure (a), HOMO (b), and LUMO (c) of inhibitor **3**.

**Table 6**  
DFT parameters of inhibitor **3** using B3LYP functional and 6-31G+(d,p) basis set.

$E_{HOMO}$ (eV)	$E_{LUMO}$ (eV)	$\Delta E$ (eV)	$IE$ (eV)	$\eta$ (eV)	$\chi$ (eV)	$\omega$ (eV)	$\sigma$ (eV)	$\Delta N$	$\mu$
-5.865	1.919	7.784	5.865	3.892	1.973	7.578	0.257	0.367	26.37

**Table 7**  
Some recently reported surfactant corrosion inhibitors of steels in acid media.

Inhibitor	Concentration	Metal/ Electrolyte (Temperature)	Inhibition efficiency (%)	References
 (DBBD)	20 mM	Mild steel/15 % HCl (25 °C)	98.0	[66]
 (MCS-14)	1 mM	API X65/3 M HCl (25 °C)	93.1	[67]
 (12-MOH-O-MOH-12)	3 mM	AISI 304 SS/3 M HCl (25 °C)	98.0	[68]
 (PMTH2E8)	4.2 mM	AISI 304 SS/3 M HCl (25 °C)	98.0	[69]
 (TMTN12Br)	3 mM	AISI 304 SS/3 M HCl (25 °C)	98.0	[70]
 (QAS-12)	0.5 mM	Q235 MS/15 % HCl (30 °C)	93.1	[71]
 (DMAEB)	100 ppm	N80 CS/15 % HCl (30 °C)	96.8	[72]
 (CGS)	200 ppm	LCS/15 % HCl (25 °C)	94.7	[73]
 (Q8Q)	13 mM	N80 steel/15 % HCl (25 °C)	95.5	[74]
 (Inhibitor <b>3</b> )	50 ppm (0.1 mM)	Mild steel/15 % HCl (30 °C)	95.2	This work

### 3.6. Mechanism of inhibition

The adsorption isotherm studies discussed earlier showed that the  $\Delta G_{ads}^{\circ}$  for the adsorption of inhibitor **3** on the mild steel surface was  $-40.19 \text{ kJ mol}^{-1}$ . This allowed us to confer that the adsorption of inhibitor **3** onto a mild steel surface follows a mixed physisorption-chemisorption mechanism. DFT studies provided a testament to this finding. Following quantum chemical calculations, HOMO and LUMO sights that interact with the metal surface through electron donation and acceptance, respectively, were revealed. It was shown that the HOMO is entirely concentrated on the chloride counter ions while the LUMO is spread over the quaternary ammonium and aromatic moieties. Fig. 11 shows how inhibitor **3** can interact with the metal surface through different functionalities embedded in the molecule. The chloride counter ions in the inhibitor, rich in electrons, can donate electrons to the empty *d*-orbitals of

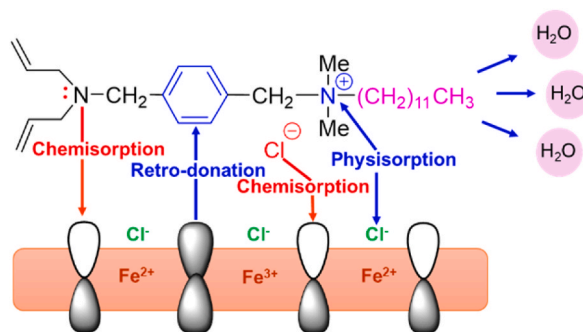


Fig. 11. A schematic representation of how inhibitor 3 interacts with mild steel surface to provide protection.

metal atoms, thereby contributing to the chemisorption nature of the overall mechanism.

On the other hand, the positively charged nitrogen ion in the quaternary ammonium moiety can afford an electrostatic interaction with the pre-adsorbed chloride ions (from 15 % HCl) on the metal surface, contributing to the physisorption nature of the overall mechanism. DFT studies showed that the aromatic ring also plays a role. Since the aromatic ring is part of the LUMO, as per the DFT study, the only way the aromatic ring could interact with the metal surface in this circumstance is through retro-donation. Retro-donation, also known as backdonation, happens when the metal atoms' filled d-orbitals donate electrons to the inhibitor's empty p-orbitals. The DFT-derived calculation of a high electrophilicity value ( $\omega$ ) supports the phenomenon of retro-donation as well. The synergism between donation ( $p\pi-d\pi$ ) and retro-donation ( $d\pi-p\pi$ ) strengthens the inhibition mechanism. Additionally, inhibitor 3 has a favorably long alkyl chain that acts as a hydrophobe. When inhibitor 3 is adsorbed on the surface, this hydrophobic alkyl chain length assists the metal surface by driving away corrosive water molecules. This was further confirmed by the water contact angle analysis discussed earlier.

### 3.6.1. Comparative inhibition performance of inhibitor 3

Some recently reported monocationic and dicationic surfactant corrosion inhibitors of steels in different HCl acid media are enumerated in Table 7. The IEs obtained from these inhibitors are all very inspiring. All reported inhibitors were tested to protect the corresponding steel structures with very high efficiency. One ubiquitous characteristic feature of these inhibitor molecules is that they all possess one/two quaternary ammonium moieties. This indicates the efficacy of quaternary ammonium compounds in arresting the corrosion of steels in acid media, which inspired the current study. A spacer between the two quaternary ammonium moieties can be entirely hydrophobic [66,72–74] or contain some heteroatoms with lone pairs [68–70] to make coordination bonds with the empty d-orbitals in the metal atoms. What makes our proposed inhibitor (inhibitor 3: the last entry in Table 7) impart such a high IE for a relatively much smaller concentration (0.1 mM, 50 ppm) than other inhibitors here is possibly a good balance between hydrophobicity, hydrophilicity, and structure simplicity. The presence of the positively charged quaternary ammonium moiety to make electrostatic interactions with the metal surface, the availability of an aromatic ring to experience retrodonation from the metal surface, nitrogen with available lone pair for chelation, and long alkyl chain length to repulse the water molecules are behind the success of the inhibitor. Other inhibitors [68–70] with similar features as inhibitor 3, at the expense of more concentration, registered similar IEs.

## 4. Conclusions

A new quaternary ammonium salt-based corrosion inhibitor 3 with hydrophobic dodecyl group and electron-rich diallylbenzyl amine moiety has been synthesized and characterized. The corrosion inhibitor was tested for suppressing mild steel corrosion in 15 % HCl at 30 °C utilizing gravimetric and electrochemical corrosion tests. Inhibitor 3 registered a very high IE of  $\approx 95.0\%$  at just 50 ppm, determined via the LPR technique. Furthermore, the IEs registered using various procedures were in close agreement and found to be 94.2, 94.7, 91.9, and 95.2 %, determined via WL, EIS, PDP, and LPR techniques. Following the effect of temperature (303–333 K) on the IE, inhibitor 3 was found to desorb slowly from the metal surface to register 91.3, 82.8, and 75.0 % IE at 40, 50, and 60 °C.  $\Delta G_{ads}^{\circ}$  A value of  $-40.19 \text{ kJ mol}^{-1}$  was determined via an isotherm study, which revealed that inhibitor 3 adsorbs via a mixed physio-chemisorption mechanism. An increase in the  $E_a$  value for blank from  $65 \text{ kJ mol}^{-1}$  to  $107.4 \text{ kJ mol}^{-1}$  for 50 ppm inhibited solution suggested a significant decrease in metal corrosion. Additionally, a steep increase in  $\Delta S_{ads}^{\circ}$  value from  $-10.3 \text{ J mol}^{-1} \text{ K}^{-1}$  for uninhibited (blank) to  $106.1 \text{ J mol}^{-1} \text{ K}^{-1}$  for inhibited solution indicated the removal of water molecules from the metal surface. DFT studies revealed the HOMO and LUMO sights that interact with the metal surface to confirm the mixed physio-chemisorption mode of adsorption. PDP studies showed that inhibitor 3 retarded the rate of mild steel corrosion by inhibiting both half-cell reactions, which was confirmed by offering discussions on the change of  $E_{corr}$  and Tafel slope values. A decrease in  $i_{corr}$  and  $R_p$  values were observed through polarization studies that confirmed the efficacy of inhibitor 3. EIS studies showed that  $R_{ct}$  values increased and  $C_{dl}$  values decreased with increasing inhibitor concentration. In-depth SEM-EDX and XPS experiments provided strong evidence for inhibitor 3 adsorption on mild steel surfaces. The water contact angle value for inhibited mild steel surface increased to  $98.7^{\circ}$  from only  $20.4^{\circ}$  for uninhibited surface, indicating inhibitor 3's excellent ability to impart hydrophobicity to mild steel surface in solution. Overall,



inhibitor **3** successfully inhibited the corrosion of mild steel in 15 % HCl at 30 °C for just a small dose of 0.1 mM (50 ppm). At a very high temperature of 60 °C, the inhibitor still showed 75.0 % IE, which is very promising. In the future, we plan to increase the IE of the inhibitor for high-temperature acid corrosion applications by modifying the hydrophobic chain length and incorporating electro-donating groups in the benzene ring. This could make the modified version of inhibitor **3** considerably less prone to desorption and will be tremendously applicable for very high temperatures.

### Data availability

The data is available upon request.

### CRedit authorship contribution statement

**Lipiar K.M.O. Goni:** Writing – original draft, Visualization, Methodology, Investigation, Formal analysis. **Shaikh A. Ali:** Writing – review & editing, Resources, Project administration, Methodology, Conceptualization. **Hasan A. Al-Muallem:** Writing – review & editing, Resources. **Mohammad A. Jafar Mazumder:** Writing – review & editing, Supervision, Resources, Methodology, Funding acquisition, Conceptualization.

### Declaration of competing interest

The authors declare no conflict of interest.

### Acknowledgements

The authors sincerely acknowledge the research facilities provided by King Fahd University of Petroleum and Minerals (KFUPM) in Saudi Arabia.

### Appendix A. Supplementary data

Supplementary data to this article can be found online at <https://doi.org/10.1016/j.heliyon.2024.e38425>.

### References

- [1] E. McCafferty, *Introduction to Corrosion Science, first ed.*, Springer-Verlag, New York, 2010.
- [2] R. Javaherdashti, How corrosion affects industry and life, *Anti-Corros Methods Mater* 47 (2000) 30–34, <https://doi.org/10.1108/00035590010310003>.
- [3] J.K. Emmanuel, Corrosion protection of mild steel in corrosive media, a shift from synthetic to natural corrosion inhibitors: a review, *Bull. Natl. Res. Cent.* 48 (2024) 26, <https://doi.org/10.1186/s42269-024-01181-7>.
- [4] J. Wang, Y. Wang, Z. Yang, L. Guo, J. Yang, Q. Yang, J. Wu, Synthesis of a novel fused heterocyclic quaternary ammonium salt and its performance in ultra-low dosage as acidizing corrosion inhibitor, *J. Mol. Struct.* 1303 (2024) 137571, <https://doi.org/10.1016/j.molstruc.2024.137571>.
- [5] G. Koch, J. Varney, N. Thompson, O. Moghissi, M. Gould, J. Payer, International measures of prevention, application, and economics of corrosion technologies study. <http://impact.nace.org/>, 2024. (Accessed 26 August 2024).
- [6] I.Y. Yaagoob, L.K.M.O. Goni, M.A.J. Mazumder, S.A. Ali, M.A. Quraishi, C. Verma, Synthesis of polymeric surfactant containing bis-cationic motifs as a highly efficient acid corrosion inhibitor for C1018 carbon steel, *New J. Chem.* 47 (2023) 3445–3461, <https://doi.org/10.1039/d2nj05978a>.
- [7] C. Verma, E.E. Ebenso, M.A. Quraishi, C.M. Hussain, Recent developments in sustainable corrosion inhibitors: design, performance and industrial scale applications, *Mater Adv* 2 (2021) 3806–3850, <https://doi.org/10.1039/d0ma00681e>.
- [8] B. Alharbi, N. Aljeaban, L.K.M.O. Goni, M.A. Jafar Mazumder, T. Chen, W. Buhaezah, S.A. Ali, Synthesis and investigation of two new compounds (2-(methoxymethyl)-1-phenyl-2-propen-1-one and 2-(methoxymethyl)-1-(4-methoxyphenyl)-2-propen-1-one) as corrosion inhibitors for mild steel in acidic solutions at elevated temperature, *Int. J. Electrochem. Sci.* 19 (2024) 100508, <https://doi.org/10.1016/j.ijoes.2024.100508>.
- [9] A.E. Al-Rawajfeh, E.M. Al-Shamailh, Inhibition of corrosion in steel water pipes by ammonium pyrrolidine dithiocarbamate (APDTC), *Desalination* 206 (2007) 169–178, <https://doi.org/10.1016/j.desal.2006.02.065>.
- [10] A.H. Nahlé, T.J. Harvey, F.C. Walsh, Quaternary aryl phosphonium salts as corrosion inhibitors for iron in HCl, *J. Alloys Compd.* 765 (2018) 812–825, <https://doi.org/10.1016/j.jallcom.2018.06.241>.
- [11] J. Haque, M.A. Jafar Mazumder, M.A. Quraishi, S.A. Ali, N.A. Aljeaban, Pyrrolidine-based quaternary ammonium salts containing propargyl and hydrophobic C-12 and C-16 alkyl chains as corrosion inhibitors in aqueous acidic media, *J. Mol. Liq.* 320 (2020) 114473, <https://doi.org/10.1016/j.molliq.2020.114473>.
- [12] N.A. Odewunmi, M.A.J. Mazumder, S.A. Ali, B.G. Alharbi, Hydroquinone decorated with alkyne, quaternary ammonium, and hydrophobic motifs to mitigate corrosion of X-60 mild steel in 15 wt.% HCl, *Chem. Asian J.* 16 (2021) 801–821, <https://doi.org/10.1002/asia.202100085>.
- [13] D.S. Chauhan, M.A. Quraishi, M.A. Jafar Mazumder, S.A. Ali, N.A. Aljeaban, B.G. Alharbi, Design and synthesis of a novel corrosion inhibitor embedded with quaternary ammonium, amide and amine motifs for protection of carbon steel in 1 M HCl, *J. Mol. Liq.* 317 (2020) 113917, <https://doi.org/10.1016/j.molliq.2020.113917>.
- [14] R. Jalab, M.A. Saad, M.H. Sliem, A.M. Abdullah, I.A. Hussein, An eco-friendly quaternary ammonium salt as a corrosion inhibitor for carbon steel in 5 M HCl solution: theoretical and experimental investigation, *Molecules* 27 (2022) 6414, <https://doi.org/10.3390/molecules27196414>.
- [15] A.S. El-Tabei, O.E. El-Azabawy, N.M. El Basony, M.A. Hegazy, Newly synthesized quaternary ammonium bis-cationic surfactant utilized for mitigation of carbon steel acidic corrosion; theoretical and experimental investigations, *J. Mol. Struct.* 1262 (2022) 133063, <https://doi.org/10.1016/j.molstruc.2022.133063>.
- [16] T. Zheng, J. Liu, M. Wang, Q. Liu, J. Wang, Y. Chong, G. Jia, Synergistic corrosion inhibition effects of quaternary ammonium salt cationic surfactants and thiourea on Q235 steel in sulfuric acid: experimental and theoretical research, *Corros Sci* 199 (2022) 110199, <https://doi.org/10.1016/j.corsci.2022.110199>.
- [17] I.R. Saad, A.M. Abdel-Gaber, G.O. Younes, B. Nsouli, Thiourea and N-methylthiourea as corrosion inhibitors for steel in phosphoric acid, *J. Fail. Anal. Prev.* 18 (2018) 1293–1299, <https://doi.org/10.1007/s11668-018-0522-5>.

- [18] M.Y. El Sayed, A.M. Abdel-Gaber, H.T. Rahal, Safranin—a potential corrosion inhibitor for mild steel in acidic media: a combined experimental and theoretical approach, *J. Fail. Anal. Prev.* 19 (2019) 1174–1180, <https://doi.org/10.1007/s11668-019-00719-6>.
- [19] I.Y. Yaagoob, L.K.M.O. Goni, C. Verma, M.A.J. Mazumder, S.A. Ali, N-(4-Chloromethylbenzyl)-N, N-dimethyldodecan-1-aminium chloride: a quaternary ammonium surfactant as corrosion inhibitor, *ChemistrySelect* 8 (2023) 483–496, <https://doi.org/10.1002/slct.202301913>.
- [20] Z. Shariatinia, A. Ahmadi-Ashtiani, Corrosion inhibition efficiency of some phosphoramidate derivatives: DFT computations and MD simulations, *J. Mol. Liq.* 292 (2019) 111409, <https://doi.org/10.1016/j.molliq.2019.111409>.
- [21] J. Sebhauy, Y. El Bakri, Y. El Aoufir, E.H. Anouar, A. Guenbour, A.A. Nasser, E. Mokhtar Essassi, Synthesis, NMR characterization, DFT and anticorrosion on carbon steel in 1M HCl of two novel 1,5-benzodiazepines, *J. Mol. Struct.* 1182 (2019) 123–130, <https://doi.org/10.1016/j.molstruc.2019.01.037>.
- [22] N. Vaszilcsin, A. Kellenberger, M.L. Dan, D.A. Duca, V.L. Ordodi, Efficiency of expired drugs used as corrosion inhibitors: a review, *Materials* 16 (2023) 5555, <https://doi.org/10.3390/ma16165555>.
- [23] T. Han, J. Guo, Q. Zhao, Y. Wu, Y. Zhang, Enhanced corrosion inhibition of carbon steel by pyridyl gemini surfactants with different alkyl chains, *Mater. Chem. Phys.* 240 (2020) 122156, <https://doi.org/10.1016/j.matchemphys.2019.122156>.
- [24] S.A. Umoren, M.M. Solomon, S.A. Ali, H.D.M. Dafalla, Synthesis, characterization, and utilization of a diallylmethylamine-based cyclopolymer for corrosion mitigation in simulated acidizing environment, *Mater Sci Eng C* 100 (2019) 897–914, <https://doi.org/10.1016/j.msec.2019.03.057>.
- [25] N.A. Odewunmi, M.A.J. Mazumder, S.A. Ali, Evaluation of 1-hexadecylbenzimidazole as a corrosion inhibitor on low carbon steel 15 % HCl solution interface, *ChemistrySelect* 6 (2021) 3199–3217, <https://doi.org/10.1002/slct.202100326>.
- [26] C. Lai, B. Xie, L. Zou, X. Zheng, X. Ma, S. Zhu, Adsorption and corrosion inhibition of mild steel in hydrochloric acid solution by S-allyl-O,O'-dialkylidithiophosphates, *Results Phys.* 7 (2017) 3434–3443, <https://doi.org/10.1016/j.rinp.2017.09.012>.
- [27] O.A. Akinbulumo, O.J. Odejobi, E.L. Odekanle, Thermodynamics and adsorption study of the corrosion inhibition of mild steel by Euphorbia heterophylla L. extract in 1.5 M HCl, *Results Mater* 5 (2020) 100074, <https://doi.org/10.1016/j.rinma.2020.100074>.
- [28] L. Afia, O. Benali, R. Salghi, E.E. Ebenso, S. Jodeh, M. Zougagh, B. Hammouti, Steel corrosion inhibition by acid garlic essential oil as a green corrosion inhibitor and sorption behavior, *Int. J. Electrochem. Sci.* 9 (2014) 8392–8406, [https://doi.org/10.1016/S1452-3981\(23\)11055-8](https://doi.org/10.1016/S1452-3981(23)11055-8).
- [29] F. Mohsenifar, H. Jafari, K. Sayin, Investigation of thermodynamic parameters for steel corrosion in acidic solution in the presence of N,N'-bis (phloracetophenone)-1,2 propanediamine, *J Bio Tribocorros* 2 (2016) 1, <https://doi.org/10.1007/s40735-015-0031-y>.
- [30] M.M. Solomon, S.A. Umoren, M.A. Quraishi, D.B. Tripathy, E.J. Abai, Effect of alkyl chain length, flow, and temperature on the corrosion inhibition of carbon steel in a simulated acidizing environment by an imidazoline-based inhibitor, *J. Pet. Sci. Eng.* 187 (2020) 106801, <https://doi.org/10.1016/j.petrol.2019.106801>.
- [31] S. Umoren, I.B. Obot, Z. Gasem, N.A. Odewunmi, Experimental and theoretical studies of red apple fruit extract as green corrosion inhibitor for mild steel in HCl solution, *J. Dispersion Sci. Technol.* 36 (2015) 789–802, <https://doi.org/10.1080/01932691.2014.922887>.
- [32] H.M. Abd El-Lateef, Corrosion inhibition characteristics of a novel salicylidene isatin hydrazine sodium sulfonate on carbon steel in HCl and a synergistic nickel ions additive: a combined experimental and theoretical perspective, *Appl. Surf. Sci.* 501 (2020) 144237, <https://doi.org/10.1016/j.apsusc.2019.144237>.
- [33] T. Han, J. Guo, Q. Zhao, Y. Wu, Y. Zhang, Enhanced corrosion inhibition of carbon steel by pyridyl gemini surfactants with different alkyl chains, *Mater. Chem. Phys.* 240 (2020) 122156, <https://doi.org/10.1016/j.matchemphys.2019.122156>.
- [34] M.T. Alhaffar, S.A. Umoren, I.B. Obot, S.A. Ali, Isoxazolidine derivatives as corrosion inhibitors for low carbon steel in HCl solution: experimental, theoretical and effect of KI studies, *RSC Adv.* 8 (2018) 1764–1777, <https://doi.org/10.1039/c7ra11549k>.
- [35] N.A. Odewunmi, S.A. Umoren, Z.M. Gasem, Utilization of watermelon rind extract as a green corrosion inhibitor for mild steel in acidic media, *J. Ind. Eng. Chem.* 21 (2015) 239–247, <https://doi.org/10.1016/j.jiec.2014.02.030>.
- [36] M.A. Moselhy, E.G. Zaki, S.A.E.H.A. El-Maksoud, M.A. Migahed, Surface activity and electrochemical behavior of some thiazine cationic surfactants and their efficiency as corrosion inhibitors for carbon steel in a sour environment, *ACS Omega* 6 (2021) 19559–19568, <https://doi.org/10.1021/acsomega.1c02005>.
- [37] O. Kharbouch, K. Dahmani, N. Errahmany, A. Belkheiri, M. Galai, F. El Hajri, A.A. Alobaid, I. Warad, S. Boukhris, M. Ebn Touhami, H. Nassali, Enhancing corrosion resistance of mild steel in 1M HCl: investigation of new benzoxazepine derivatives through synthesis, electrochemical analysis, surface analysis, XPS, DFT, and molecular dynamics simulation, *ChemistrySelect* 9 (2024) e202303045, <https://doi.org/10.1002/slct.202303045>.
- [38] A. Khanra, R.N. Gayen, Distribution of relaxation time in solution-processed polycrystalline CZTS thin films: study of impedance spectroscopy, *Ceram. Int.* 44 (2018) 14095–14100, <https://doi.org/10.1016/j.ceramint.2018.05.007>.
- [39] N. Arousse, Y. Fernine, N. Al-Zaqri, A. Boshala, E. Ech-Chihbi, R. Salim, F. El Hajjaji, A. Alami, M.E. Touhami, M. Taleb, Thiophene derivatives as corrosion inhibitors for 2024-T3 aluminum alloy in hydrochloric acid medium, *RSC Adv.* 12 (2022) 10321–10335, <https://doi.org/10.1039/d2ra00185c>.
- [40] S.A. Xavier Stango, U. Vijayalakshmi, Studies on corrosion inhibitory effect and adsorption behavior of waste materials on mild steel in acidic medium, *J Asian Ceramic Soc.* 6 (2018) 20–29, <https://doi.org/10.1080/21870764.2018.1439608>.
- [41] S. Hosny, A. Abdelfatah, G.A. Gaber, Synthesis, characterization, synergistic inhibition, and biological evaluation of novel Schiff base on 304 stainless steel in acid solution, *Sci. Rep.* 14 (2024) 470, <https://doi.org/10.1038/s41598-023-51044-w>.
- [42] S. Shao, B. Wu, P. Wang, P. He, X.P. Qu, Investigation on inhibition of ruthenium corrosion by glycine in alkaline sodium hypochlorite based solution, *Appl. Surf. Sci.* 506 (2020) 144976, <https://doi.org/10.1016/j.apsusc.2019.144976>.
- [43] V. Kalia, P. Kumar, S. Kumar, M. Goyal, P. Pahuja, G. Jhaa, S. Lata, H. Dahiya, S. Kumar, A. Kumari, C. Verma, Synthesis, characterization and corrosion inhibition potential of oxadiazole derivatives for mild steel in 1M HCl: electrochemical and computational studies, *J. Mol. Liq.* 348 (2022) 118021, <https://doi.org/10.1016/j.molliq.2021.118021>.
- [44] S. Kumar, V. Kalia, M. Goyal, G. Jhaa, S. Kumar, H. Vashisht, H. Dahiya, M.A. Quraishi, C. Verma, Newly synthesized oxadiazole derivatives as corrosion inhibitors for mild steel in acidic medium: experimental and theoretical approaches, *J. Mol. Liq.* 357 (2022) 119077, <https://doi.org/10.1016/j.molliq.2022.119077>.
- [45] A.A. Al-Amiery, A.B. Mohamad, A.A.H. Kadhum, L.M. Shaker, W.N.R.W. Isahak, M.S. Takriff, Experimental and theoretical study on the corrosion inhibition of mild steel by nonanedioc acid derivative in hydrochloric acid solution, *Sci. Rep.* 12 (2022) 4705, <https://doi.org/10.1038/s41598-022-08146-8>.
- [46] A.F.S. Abdul Rahiman, S. Sethumanickam, Corrosion inhibition, adsorption and thermodynamic properties of poly(vinyl alcohol-cysteine) in molar HCl, *Arab. J. Chem.* 10 (2017) S3358–S3366, <https://doi.org/10.1016/j.arabjc.2014.01.016>.
- [47] Z. Lakbaibi, M. Damej, A. Molhi, M. Benmessoud, S. Tighadouini, A. Jaafar, T. Benabbouha, A. Ansari, A. Driouch, M. Tabyaoui, Evaluation of inhibitive corrosion potential of symmetrical hydrazine derivatives containing nitrophenyl moiety in 1M HCl for C38 steel: experimental and theoretical studies, *Heliyon* 8 (2022) e09087, <https://doi.org/10.1016/j.heliyon.2022.e09087>.
- [48] M. Damej, A. Molhi, K. Tassouli, B. El Ibrahim, Z. Akounach, A.A. Addi, S. El hajjaji, M. Benmessoud, Experimental and theoretical study to understand the adsorption process of p-anisidine and 4-nitroaniline for the dissolution of c38 carbon steel in 1M HCl, *ChemistrySelect* 7 (2022) e202103192, <https://doi.org/10.1002/slct.202103192>.
- [49] L.W. El Khatib, H.T. Rahal, A.M. Abdel-Gaber, Synergistic effect between fragaria ananassa and cucurbita pepo l leaf extracts on mild steel corrosion in hydrochloric acid solutions, *Prot Chem Phys Met Surf.* 56 (2020) 1096–1106, <https://doi.org/10.1134/S2070205120050111>.
- [50] R.S. Al-Moghrabi, A.M. Abdel-Gaber, H.T. Rahal, A comparative study on the inhibitive effect of Crataegus oxyacantha and Prunus avium plant leaf extracts on the corrosion of mild steel in hydrochloric acid solution, *Int J Ind Chem.* 9 (2018) 255–263, <https://doi.org/10.1007/s40090-018-0154-3>.
- [51] B. Andrzejewski, K. Chybczyńska, B. Hilczer, M. Błaszczak, T. Luciński, M. Matczak, L. Kępiński, Controlled growth of bismuth ferrite multiferroic flowers. <https://arxiv.org/abs/1402.1336v>, 2014. (Accessed 26 August 2024).
- [52] D. Wilson, M.A. Langell, XPS analysis of oleylamine/oleic acid capped Fe<sub>3</sub>O<sub>4</sub> nanoparticles as a function of temperature, *Appl. Surf. Sci.* 303 (2014) 6–13, <https://doi.org/10.1016/J.APSUSC.2014.02.006>.
- [53] P.K. Paul, M. Yadav, Investigation on corrosion inhibition and adsorption mechanism of triazine-thiourea derivatives at mild steel/HCl solution interface: electrochemical, XPS, DFT and Monte Carlo simulation approach, *J. Electroanal. Chem.* 877 (2020) 114599, <https://doi.org/10.1016/J.JELECHEM.2020.114599>.

- [54] Y. Gu, S. Chen, J. Ren, Y.A. Jia, C. Chen, S. Komarneni, D. Yang, X. Yao, Electronic structure tuning in Ni<sub>3</sub>FeN/r-GO aerogel toward bifunctional electrocatalyst for overall water splitting, *ACS Nano* 12 (2018) 245–253, <https://doi.org/10.1021/acsnano.7b05971>.
- [55] N.C.T. Martins, J. Angelo, A.V. Girão, T. Trindade, L. Andrade, A. Mendes, N-doped carbon quantum dots/TiO<sub>2</sub> composite with improved photocatalytic activity, *Appl. Catal., B* 193 (2016) 67–74, <https://doi.org/10.1016/j.apcatb.2016.04.016>.
- [56] J. Cao, Y. Wang, J. Chen, X. Li, F.C. Walsh, J.-H. Ouyang, D. Jia, Y. Zhou, Three-dimensional graphene oxide/polypyrrole composite electrodes fabricated by one-step electrodeposition for high-performance supercapacitors, *J Mater Chem A Mater* 3 (2015) 14445–14457, <https://doi.org/10.1039/C5TA02920A>.
- [57] N.Z.N. Hashim, E.H. Anouar, K. Kassim, H.M. Zaki, A.I. Alharthi, Z. Embong, XPS and DFT investigations of corrosion inhibition of substituted benzylidene Schiff bases on mild steel in hydrochloric acid, *Appl. Surf. Sci.* 476 (2019) 861–877, <https://doi.org/10.1016/J.APSUSC.2019.01.149>.
- [58] S. Ralkhal, T. Shahrabi, B. Ramezanzadeh, G. Bahlakeh, A combined electrochemical, molecular dynamics, quantum mechanics and XPS analysis of the mild steel surface protected by a complex film composed of neodymium (III) and benzimidazole, *Appl. Surf. Sci.* 464 (2019) 178–194, <https://doi.org/10.1016/J.APSUSC.2018.09.064>.
- [59] P. Singh, V. Srivastava, M.A. Quraishi, Novel quinoline derivatives as green corrosion inhibitors for mild steel in acidic medium: electrochemical, SEM, AFM, and XPS studies, *J. Mol. Liq.* 216 (2016) 164–173, <https://doi.org/10.1016/J.MOLLIQ.2015.12.086>.
- [60] N.S. Abdelsafi, A.A. Farag, F.E.T. Heakal, A.S. Badran, K.M. Abdel-Azim, A.R. Manar El Sayed, M.A. Ibrahim, In-depth experimental assessment of two new aminocoumarin derivatives as corrosion inhibitors for carbon steel in HCl media combined with AFM, SEM/EDX, contact angle, and DFT/MDs simulations, *J. Mol. Struct.* 1304 (2024) 137638, <https://doi.org/10.1016/j.molstruc.2024.137638>.
- [61] E. Gutiérrez, J.A. Rodríguez, J. Cruz-Borbolla, J.G. Alvarado-Rodríguez, P. Thangarasu, Development of a predictive model for corrosion inhibition of carbon steel by imidazole and benzimidazole derivatives, *Corros Sci* 108 (2016) 23–35, <https://doi.org/10.1016/J.CORSCI.2016.02.036>.
- [62] M. Esmailzadeh Khabazi, A. Najafi Chermahini, DFT study on corrosion inhibition by tetrazole derivatives: investigation of the substitution effect, *ACS Omega* 8 (2023) 9978–9994, <https://doi.org/10.1021/acsomega.2c07185>.
- [63] Z. Lai, S. Wang, C. Wang, Y. Hong, G. Zhou, Y. Chen, W. He, Y. Peng, D. Xiao, A comparison of typical additives for copper electroplating based on theoretical computation, *Comput. Mater. Sci.* 147 (2018) 95–102, <https://doi.org/10.1016/J.COMMATSCI.2017.11.049>.
- [64] H. Bourzi, R. Oukhrif, B. El Ibrahim, H.A. Oualid, Y. Abdellaoui, B. Balkard, M. Hilali, S. El Issami, Understanding of anti-corrosive behavior of some tetrazole derivatives in acidic medium: adsorption on Cu (111) surface using quantum chemical calculations and Monte Carlo simulations, *Surf. Sci.* 702 (2020) 121692, <https://doi.org/10.1016/J.SUSC.2020.121692>.
- [65] I. Abdulazeez, M. Khaled, A.A. Al-Saadi, Impact of electron-withdrawing and electron-donating substituents on the corrosion inhibitive properties of benzimidazole derivatives: a quantum chemical study, *J. Mol. Struct.* 1196 (2019) 348–355, <https://doi.org/10.1016/J.MOLSTRUC.2019.06.082>.
- [66] D. Wang, Y. Li, B. Chen, L. Zhang, Novel surfactants as green corrosion inhibitors for mild steel in 15% HCl: experimental and theoretical studies, *Chem Eng J* 402 (2020) 126219, <https://doi.org/10.1016/j.cej.2020.126219>.
- [67] A.A. Farag, H.E. Abdallah, E.A. Badr, E.A. Mohamed, A.I. Ali, A.Y. El-Etre, The inhibition performance of morpholinium derivatives on corrosion behavior of carbon steel in the acidized formation water: theoretical, experimental and biocidal evaluations, *J. Mol. Liq.* 341 (2021) 117348, <https://doi.org/10.1016/j.molliq.2021.117348>.
- [68] O. Kaczerewska, R. Leiva-Garcia, R. Akid, B. Brycki, I. Kowalczyk, T. Pospieszny, Effectiveness of O-bridged cationic gemini surfactants as corrosion inhibitors for stainless steel in 3 M HCl: experimental and theoretical studies, *J. Mol. Liq.* 249 (2018) 1113–1124, <https://doi.org/10.1016/j.molliq.2017.11.142>.
- [69] M. Pakiet, I. Kowalczyk, R. Leiva Garcia, R. Akid, B. Brycki, Cationic cleavable surfactants as highly efficient corrosion inhibitors of stainless steel AISI 304: electrochemical study, *J. Mol. Liq.* 315 (2020) 113675, <https://doi.org/10.1016/j.molliq.2020.113675>.
- [70] M. Pakiet, I.H. Kowalczyk, R. Leiva Garcia, R. Akid, B.E. Brycki, Influence of different counterions on gemini surfactants with polyamine platform as corrosion inhibitors for stainless steel AISI 304 in 3 M HCl, *J. Mol. Liq.* 268 (2018) 824–831, <https://doi.org/10.1016/j.molliq.2018.07.120>.
- [71] A.O. Alnajjar, H.M. Abd El-Lateef, A novel approach to investigate the synergistic inhibition effect of nickel phosphate nanoparticles with quaternary ammonium surfactant on the Q235-mild steel corrosion: surface morphology, electrochemical-computational modeling outlines, *J. Mol. Liq.* 337 (2021) 116125, <https://doi.org/10.1016/j.molliq.2021.116125>.
- [72] M.A. Deyab, Q. Mohsen, Inhibitory influence of cationic Gemini surfactant on the dissolution rate of N80 carbon steel in 15% HCl solution, *Sci. Rep.* 11 (2021) 10521, <https://doi.org/10.1038/s41598-021-90031-x>.
- [73] N.D. Mu'azu, S.A. Haladu, J.M. AlGhamdi, H.A. Alqahtani, M.S. Manzar, M. Zubair, N.A. Odewunmi, N.E. Aldossary, H. Saud alareefi, Z.H. Alshaer, S.A. Ali, H. M.A. El-Lateef, Inhibition of low carbon steel corrosion by a cationic gemini surfactant in 10wt.% H<sub>2</sub>SO<sub>4</sub> and 15wt.% HCl under static condition and hydrodynamic flow, *S. Afr. J. Chem. Eng.* 43 (2023) 232–244, <https://doi.org/10.1016/j.sajce.2022.10.006>.
- [74] X. Zhang, Y. Zheng, X. Wang, Y. Yan, W. Wu, Corrosion inhibition of N80 steel using novel diquaternary ammonium salts in 15% hydrochloric Acid, *Ind. Eng. Chem. Res.* 53 (2014) 14199–14207, <https://doi.org/10.1021/ie502405a>.